CHARLES UNIVERSITY

FACULTY OF SCIENCE

Study Programme: Biochemistry

BSc. Celeste de Sousa Santos Abreu

INTERACTION OF GALECTIN-1 WITH HUMAN NK CELL RECEPTORS

INTERAKCE GALEKTINU-1 S RECEPTORY LIDSKÝCH NK BUNĚK

Master's Thesis

Supervisor: RNDr. Ondřej Vaněk, Ph.D.

Prague 2019

Statement of authorship

I hereby declare that I am the sole author of this Master's thesis and that I have worked under the supervision of RNDr. Ondřej Vaněk, Ph.D. All referenced literature has been properly cited throughout the text and in the references. I further declare that I have not submitted this thesis at any other institution with the intent of obtaining an academic title.

Prague, 18th of August 2019

Signature: _____

BSc. Celeste Abreu

Acknowledgments

I would like to thank RNDr. Ondřej Vaněk, Ph.D. for the opportunity given to join the laboratory and work in this project, and for providing valuable insights and guidance throughout my Master's degree. Additional thanks should also be given for the measurement and evaluation of AUC data.

To RNDr. Jan Bláha, Ph.D., I would also like to express my gratitude for all the availability to discuss the project and for all the brainstorming sessions that proved most valuable in the development of the work done. I would also like to thank Mgr. Barbora Kalousková, Mgr. Ondřej Skořepa, and Mgr. Samuel Pažický for all the training and valuable knowledge shared, and the remaining members of Laboratory 204 for being great colleagues throughout these years.

I would additionally like to thank Ing. Jan Dohnálek, Ph.D., for so kindly welcoming me to BIOCEV for the biophysical measurements included in this thesis. I would also like to acknowledge the training and guidance provided by Mgr. Tomáš Kovaľ, Ph.D. for MST and to thank Tatsiana Charnavets, Ph.D., for all the advice given during the biophysical experiments.

Very importantly, I would like to thank my closest friends and family who have always been there for me when most needed.

To my parents João and Maria, my aunt Amélia, and D. Maria do Carmo, I would like to express my most heartfelt and sincere thank you for allowing me to a create a path for myself whilst always being present and supportive.

This work was supported by BIOCEV (ERDF CZ.1.05/1.1.00/02.0109), Czech Science Foundation (18-10687S), and MEYS of the Czech Republic (LTC17065 within the COST Action CA15126).

Abstract

Natural killer (NK) cells are a subpopulation of effector lymphocytes with cytotoxic activity and cytokine-producing functions considered as an integral part of the innate immune response. Functions of NK cells include tumour elimination, engagement and regulation of antiviral immune responses and regulation of immune cells by production and secretion of chemokines and cytokines.

CD69 is a C-type lectin-like transmembrane receptor expressed in NK cells. CD69 is an activating receptor and acts also as a very early marker of lymphocyte activation. Putative protein ligands have been described for CD69 in the last years: Galectin-1, $S1P_1$, S100A8/S100A9 and Myl9/12. Galectin-1 is a prototypical lectin characterized by the presence of a common lectin structural fold and a carbohydrate recognition domain involved in carbohydrate binding. Galectin-1 was identified as a binding partner for CD69 based on biological and functional studies, but structural details about the complex are still missing.

This thesis describes the successful establishment of an expression protocol for a tag-less cysteine-less mutant of galectin-1 and the study of the interaction between galectin-1 and NK cell receptors. The interaction was studied using microscale thermophoresis and confirmed as dependent on the presence of a N-glycan moiety on the NK cell receptor surface.

Key-words: NK cell, CD69, Galectin-1, glycosylation, microscale thermophoresis

Abstrakt

Přirozeně zabíječské buňky (z anglického natural killer cells) jsou subpopulace efektorových lymfocytů, které mají cytotoxickou aktivitu a schopnost produkovat cytokiny, považované za nedílnou součást vrozené imunitní odpovědi. Funkce NK buněk zahrnují eliminaci nádoru, zapojení a regulaci antivirových imunitních odpovědí a regulaci imunitních buněk produkcí a sekrecí chemokinů a cytokinů.

CD69 je transmembránový receptor podobný lektinům typu C exprimovaný v NK buňkách. CD69 je aktivačním receptorem NK buněk a slouží jako velmi časný marker aktivace lymfocytů. V posledních letech byly popsány předpokládané proteinové ligandy CD69: Galektin-1, $S1P_1$, S100A8/S100A9 a Myl9/12. Galektin-1 je typický lektin charakterizovaný přítomností společného lektinového strukturního motivu a domény rozpoznávající a podílející se na vazbě sacharidů. Galektin-1 byl identifikován jako vazebný partner pro CD69 na základě biologických a funkčních studií, ale strukturální podrobnosti o komplexu stále chybí.

Tato práce popisuje úspěšné zavedení protokolu pro expresi mutované formy galektinu-1 neobsahující cysteiny ani purifikační kotvu a studium interakce mezi galektinem-1 a receptory NK buněk. Interakce byla studovaná mikrotermoforézou a byla popsána jako závislá na přítomnosti N-vázané glykosylace na povrchu receptoru.

Klíčová slova: NK buňky, CD69, Galektin-1, glykosylace, mikrotermoforézy

Table of contents

Abbreviations

AA	Acrylamide
APS	Ammonium persulfate
AUC	Analytical ultracentrifugation
bp	Base pair
BSA	Bovine serum albumin
CBB R-250	Coomassie brilliant blue R-250 dye
CD	Cluster of differentiation
CD69	Cluster of differentiation 69
CLR	C-type lectin receptor
CRD	Carbohydrate recognition domain
CTLD	C-type lectin-like domain
DC	Dendritic cell
ddH_2O	Double-deionized water
DLS	Dynamic light scattering
DNA	Deoxyribonucleic acid
dNTP	Deoxyribonucleotide triphosphate
DSF	Differential scanning fluorimetry
EDTA	Ethylenediaminetetraacetic acid
$GnTI^-$	N-acetylglucosaminyltransferase I negative
GPCR	G protein-coupled receptor
HEK293	Human embryonic kidney 293
HPLC	High-performance liquid chromatography
HSC	Hematopoietic stem cell
IFN-γ	Interferon gamma
IL	Interleukin
IPTG	Isopropyl β-D-1-thiogalactopyranoside
ITAM	Immunoreceptor tyrosine-based activation motif
ITIM	Immunoreceptor tyrosine-based inhibitory motif
KACL	Keratinocyte-associated C-type lectin
KIR	Killer immunoglobulin receptor

LB	Lysogeny broth
LLT1	Lectin-like transcript-1
lPEI	Linear polyethylenimine
LRC	Leukocyte receptor complex
MHC	Major histocompatibility complex
MST	Microscale thermophoresis
Myl	Myosin light chain
NCR	Natural cytotoxicity receptor
NK	Natural killer
NKC	Natural killer complex
NKG2D	Natural killer group 2D
NKp30	Natural cytotoxicity receptor 30
PBS	Phosphate-buffered saline
PCR	Polymerase chain reaction
PMSF	Phenylmethylsulphonyl fluoride
$S1P_1$	Sphingosine 1-phosphate receptor-1
SDS	Sodium dodecyl sulphate
SDS-PAGE	Sodium dodecyl sulphate polyacrylamide gel electrophoresis
TAE	Tris-acetate-EDTA
TEMED	Tetramethylethylenediamine
TES	Tris-EDTA-sodium chloride
TNF	Tumour necrosis factor
TRAIL	TNF-related apoptosis-inducing ligand
Tris	Tris(hydroxymethyl)aminomethane

1. Introduction

1.1. Immune system

Vertebrates are continuously exposed to organisms capable of threatening the integrity of the host by an array of mechanisms (Parkin and Cohen, 2001). The immune system has evolved to protect the host from infective pathogens whilst also maintaining host integrity by self and nonself discrimination. The response of mammalian immune system can be divided into two types: innate and adaptive. Innate immunity is comprised of physical, chemical and microbiological barriers, and a variety of myeloid and lymphoid cells able of providing immediate defence in the event of pathogenicity through a repertoire of germline-encoded receptors (Turvey and Broide, 2010). Adaptive immune responses are based on the expression of antigen-specific receptors on T and B lymphocytes that are generated by somatic recombination of germ line-encoded elements thus resulting in a highly specific and tailor-made response (Bonilla and Oettgen, 2010). Despite fundamental differences in the mechanisms of action, interaction between innate and adaptive immune systems is crucial for mounting a fully effective response as well as for maintaining host immune homeostasis (Clark and Kupper, 2005).

1.2. Natural killer cells

Natural killer (NK) cells are a subpopulation of effector lymphocytes of the innate immunity with cytotoxic activity and cytokine-producing effector function (Topham and Hewitt, 2009). NK cells contribute to innate immunity by recognizing and inducing the death of auto-reactive, virus-infected, and tumour cells in the absence of specific immunization. NK cells have also been described as major producers of cytokines and chemokines in physiological and pathological conditions. Most notably, NK cells produce tumour necrosis factor-α (TNF- α), interferon- γ (IFN-γ), several interleukins (IL)-5, -10, and -13, and an array of chemokines (Fauriat et al., 2010).

The mechanism of NK cell cytotoxicity was first proposed by Ljunggren and Kärre in the "missing self" hypothesis (Ljunggren and Kärre, 1990). The hypothesis proposed that NK cells recognize and engage into killing of any target with absent or reduced expression of self-major histocompatibility (MHC) class I molecules (whether caused by mutation, malignant transformation, arrest in differentiation or viral infection) (Ljunggren and Kärre, 1990). The hypothesis has been confirmed and extended by experimental data. Currently it

is known that MHC class I recognition on target cells by NK cell inhibitory receptors results in the inhibition of NK cells cytotoxicity. Conversely, NK cells engage into killing when there is a lack of engagement between NK cell inhibitory receptors and target MHC class I molecules (Topham and Hewitt, 2009) (Figure 1).

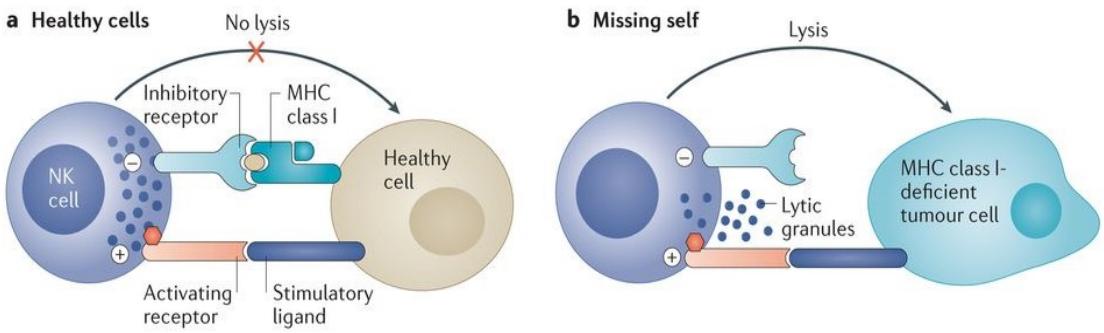

Figure 1 – Schematic representation of natural killer cell recognition. NK cell surveillance occurs via the recognition of self MHC class I molecules constitutively expressed on the surface of target cells. (A) The engagement with self MHC class I molecules on the target cell inform the NK cell that no cytotoxic attack is to be employed. Nevertheless, NK cell cytotoxicity is regulated via a dynamic equilibrium between activating and inhibitory signalling by the NK receptor interaction with cognate ligands on target cells. **(B)** Representation of "missing-self" hypothesis, where NK cells detect an absent or downregulated MHC class I molecules in the target cells thus engaging into a cytotoxic attack resulting in the programmed death of the recognized cell. Adapted from (Morvan and Lanier, 2016)

Natural killer cells have been extensively described as able to engage into cytotoxicity without the need for priming, contrarily to what is known for other effector lymphocytes (Herberman et al., 1975). However, several studies proposed the need of an interaction with dendritic cells (DCs) for NK cell activation. A detailed mechanistic description was proposed by Lucas and colleagues (Lucas et al., 2007). In a combination of *in vitro* and *in vivo* studies, the authors showed that naïve NK cells display negligible levels of cytotoxicity against target cells in the absence of priming by dendritic cells. Further description of priming location and requirements was also presented: priming occurs primarily in secondary lymphoid tissues and it is dependent on constitutive expression of IL-15/IL-15α by dendritic cells (Lucas et al., 2007).

1.2.1. Development of NK cells

Natural killer cells originate from bone marrow-derived hematopoietic stem cells (HSCs), similarly to all cells of the hematopoietic system (Kondo et al., 2001). For decades it was

generally accepted that NK cell generation and development occurred exclusively in the bone marrow (Blom and Spits, 2006). Numerous recent studies have demonstrated that NK cell precursors can additionally be found in extramedullary tissues such as in secondary lymphoid tissues (Fehniger et al., 2003; Freud et al., 2005); however, the identification of NK precursors outside of the bone marrow does not necessarily prove that development can also occur in those tissues (Blom and Spits, 2006).

Colucci and colleagues proposed a three-stage model for NK cell development based on advances made in the identification of the developmental stages involved in lymphocyte generation and in the description of hematopoietic precursor formation (Colucci et al., 2003). The model is subdivided into three main stages: (i) initial commitment of HSCs to the lymphoid lineage followed by commitment to NK cell lineage; (ii) maturation of NK precursor to NK cell by receptor repertoire selection; and (iii) export of mature NK cells to peripheral organs.

The first proposed stage involves commitment of HSCs first to the lymphoid lineage and second to the NK cell lineage. Commitment to NK cell lineage appears to be driven by expression of cytokine-dependent receptors, by the direct involvement of cytokines, and by regulation of transcription factors at the gene level. Maturation of NK precursors to NK cells is described in the second stage of the mechanism. NK cell maturation is initiated by expression of NK cell receptors in a sequential manner starting by receptors of the C-type lectin family and followed by expression of MHC-specific receptors. In addition to receptor acquisition, NK cells also develop self-tolerance as well as their cytolytic and cytokine-producing capacities. Mature NK cells are then exported to several tissues, including spleen, lung, intestine and placenta. In addition, they can be also found in circulation. The mechanism that directs NK cells to peripheral organs under normal conditions has yet to be fully described (Colucci et al., 2003).

Human natural killer cells can be subdivided into two subsets with differential abundance of surface CD56 and functions: $CD56^{dim}$ and $CD56^{bright}$ NK cell subsets, differing in specialization and location. Approximately 90% of NK cells in peripheral blood and spleen are $CD56^{dim}CD16^{+}$. This subset of NK cells is characterized by expression of perforin and thus higher cytotoxic activity, and by expression of IFN-γ after interaction with tumour cells *in vitro* (Moretta, 2010). On the contrary, $CD56^{bright}CD16^{-}$ NK cells constitute a minor NK cell subpopulation found predominantly in lymph nodes and tonsils. This NK cell subset has

poor cytolytic activity due to the absence of perforin expression; however, they readily produce cytokines such as IFN-γ, TNF-α, IL-10, and IL-13 (Poli et al., 2009).

NK cells are considered to bridge innate and adaptive immunity by modulating immunoregulatory processes by their known roles in cytokine and chemokine expression. Functional studies using mouse models have additionally shown that NK cells can acquire adaptive immunity-like properties such as memory and antigen-specific secondary responses, thus reinforcing the idea of NK cells as an evolutionary link between innate and adaptive immunity (Sun and Lanier, 2009).

1.2.2. Functions of NK cells

NK cells were originally described as large granular lymphocytes with natural cytotoxicity against tumour cells. NK cells were later recognized as a separate lymphocyte subpopulation with both cytotoxicity and cytokine-producing effector functions. NK cells are currently known as effector lymphocytes involved in tumour and autoreactive cell elimination and engagement into and regulation of antiviral immune responses, whilst also exhibiting regulatory functions thus limiting or exacerbating immune responses (Vivier et al., 2008).

Involvement of natural killer cells in cancer immunosurveillance and elimination, as well as in early defence against viruses has been strongly supported by experimental evidence obtained in functional *in vitro* and *in vivo* studies. *In vivo* studies using mice have previously proved the role of NK-cell mediated elimination of tumour cells and in mediation of cytokine expression. Comparative analysis of NK cell function in humans has been hampered by the scarcity of NK cell-selective deficiencies; nevertheless, results from an epidemiologic survey have shown that low NK cell activity is associated with increased risk of cancer (Imai et al., 2000). Compelling evidence for the role of NK cells in antiviral immune responses has been reported in a study in which a higher susceptibility to herpesvirus MCMV occurred after NK cell depletion (Lee et al., 2007). NK cells appear to reduce the risk of development of inflammatory disorders by controlling the infections and thus the immunopathology (Vivier et al., 2008).

In addition to cytotoxic activity, NK cells also act as regulatory agents in the modulation of various other cell, such as dendritic cells, T lymphocytes, B lymphocytes, and endothelial cells, by secretion of cytokines, chemokines, and growth factors. NK cell interaction with DCs in peripheral tissues influences DC homeostasis and maturation by secretion of IFN-γ

and TNF-α – a mechanism that in turn activates NK cells by means of IL-2 (Ferlazzo et al., 2002). NK cell-based modulation of adaptive immune cells protects the host against excessive responses by T and B lymphocytes thus explaining the previously reported role of NK cells in autoimmunity. In endothelial cells, NK cells have been reported in the remodelling of the feeding arterial systems by secretion of vascular endothelial growth factor and placental growth factor which are involved in mechanisms of angiogenesis, occurring for example during pregnancy. NK cell involvement with endothelial cells can also result in pathogenicity, as shown during protocols of xenotransplantation or during pathogenesis of vascular injury (Figure 2) (Hanna et al., 2006).

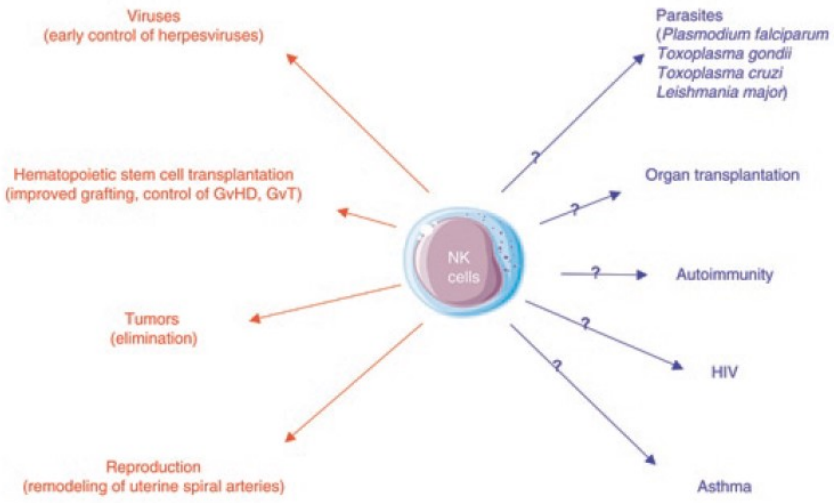

Figure 2 – Functions of natural killer cells. Involvement of NK cells in tumour immunosurveillance and elimination, and control of antiviral immune responses has been extensively reported *in vitro* and *in vivo* studies. NK cells additionally play an important role in promoting angiogenesis of uterine spiral arteries during pregnancy. Possible anti-rejection activity appears to improve grafting in HSC transplantation. The known biological roles of NK cells are shown in red; the suspected functions, in blue (Vivier et al., 2008).

1.2.3. NK cell cytotoxicity

Under normal circumstances of immune surveillance, human NK cells have inhibitory and activating receptors that recognize cognate ligands on virtually every cell in the body. The engagement of these receptors regulates NK cell activities. The dynamic equilibrium between activating and inhibitory signalling dictates whether NK cells engage into killing or not.

After activation, NK cell responses are marked by robust proliferation and synthesis of proinflammatory cytokines and cytotoxic machinery (Figure 3, page 17) (Poznanski and Ashkar, 2019). Subsequent to target recognition, NK cells engage into killing via an array of different pathways, all resulting in induction of apoptosis of the target cell. The first pathway involves the Ca^{2+}-dependent exocytosis of cytotoxic granules storing perforin and granzymes. The second pathway occurs via the death ligand/death receptor system and has been implicated in tumour surveillance and regulation of autoimmunity, in addition to its known role in apoptosis (Diehl et al., 2004).

The perforin/granzyme cell death pathway is initiated upon target cell recognition by a sequential mechanism that terminates by secretory lysosome exocytosis and release of granzymes and perforin. This mechanism can be subdivided into four main stages: (i) formation of immunological synapse at the point of contact with the target cell and cytoskeleton rearrangement; (ii) polarization of NK cell microtubule-organizing centre towards the lytic synapse; (iii) docking of lysosome with plasma membrane at the lytic synapse; and (iv) lysosome fusion with the plasma membrane and release of cytotoxic contents (Topham and Hewitt, 2009). Release of perforin into the immunological synapse causes the formation of a pore in the target cell membrane, thus allowing the entry of granzymes into the target cell. Granzymes induce target cell death through diverse pathways; granzyme B is a pro-apoptotic granzyme that cleaves target cell proteins, in a manner similar to that of caspases, thus imposing death in an effective and prompt way (5-8 minutes). Granzyme A promotes death in a caspase-independent manner providing an alternative mechanism for cells resistant to caspase or granzyme B activity (Lieberman, 2010; Voskoboinik et al., 2015).

The death receptor pathway is comprised of both Fas/FasL- and TRAIL-induced apoptosis. The first mechanism is dependent on the engagement and cross-linking of Ca^{2+}-independent Fas ligand expressed on target cells with their cognate Fas ligand constitutively expressed on the NK cell surface. The second mechanism is mediated via expression and release of TNF- α-mediated apoptosis inducing-ligand (TRAIL) (Smyth et al., 2005; Zamai et al., 1998) by NK cells, followed by binding to its cognate receptor through the recruitment of FAS-associated protein with death domain. This interaction promotes the recruitment of a range of caspases, thus promoting the formation of a multi-protein complex on the cell membrane. Concerted action of caspases results in cleaving of numerous cellular proteins,

culminating in apoptosis (Johnstone et al., 2008). The TRAIL death receptor pathway is highly induced in NK cells upon IL-2, IFNs, and IL-15 stimulation. In addition to proapoptotic activities, TRAIL can activate diverse intracellular signalling pathways that stimulate cell survival and proliferation (Johnstone et al., 2008; Sheard et al., 2013; Smyth et al., 2005).

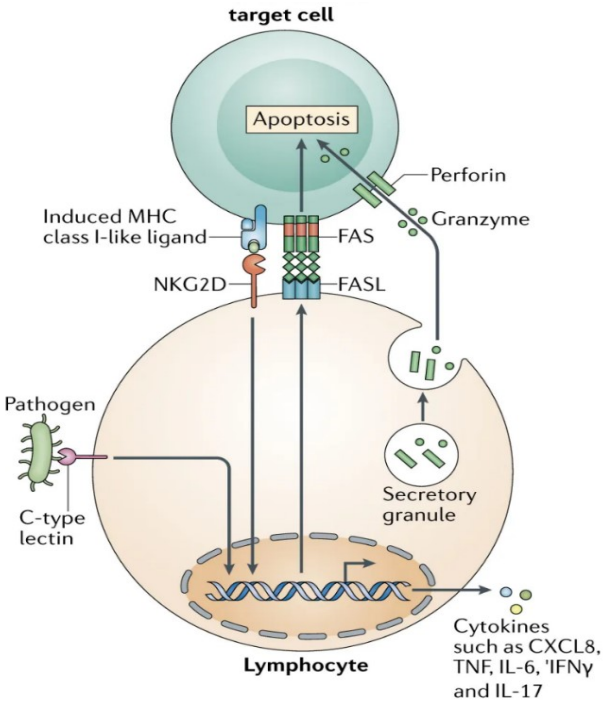

Figure 3 – Representation of lymphocyte cytotoxicity and cytokine secretion. Surveillance of the target cell by sensing changes in MHC class I and MHC class I-like molecules occur via engagement with NK cell receptor NKG2D. Recognition of an impaired expression of MHC ligands on the target cell triggers a proinflammatory response by the NK cell resulting in enhanced expression of inflammatory cytokines and chemokines and cytotoxic machinery. Target cell death occurs via a Ca^{2+}-dependent exocytosis of granules containing perforin and granzymes, or via Fas/FasL death receptor pathway. Direct recognition of pathogen ligands by C-type lectin and C-type lectin-like receptors on the NK cell surface also result in production of proinflammatory effector molecules (e.g., TNF, CXCL8, IFN-γ, and IL-17). Adapted from (Brown et al., 2018).

1.2.4. NK cell receptors

Natural killer cell recognition and cytotoxicity against target cells is controlled by the expression of activating and inhibitory receptors encoded in two main gene clusters: the natural killer complex (NKC), and the leukocyte receptor complex (LRC) (Trowsdale, 2001). The cytotoxicity is regulated through the balance between inhibiting and activating

signalling perceived from the interaction between the NK cell receptor and target cell ligand (Diefenbach and Raulet, 2001; Moretta et al., 2006).

NK cell activating and inhibitory receptors use opposing signalling motifs to promote or inhibit activation (Pegram et al., 2011). Activating receptors signal through immunoreceptor tyrosine-based activating motifs (ITAMs) located in the cytoplastic domain. ITAM-receptor activation has been described to trigger a signal cascade, thus stimulating degranulation by promoting cytoskeleton rearrangement, and transcription of genes encoding for cytokines and chemokines (Tomasello et al., 2000). On the contrary, inhibitory receptors signal through intracellular immunoreceptor tyrosine-based inhibitory motifs (ITIMs) located in the cytoplasmic tails. Inhibitory receptors recruit phosphatases to the NK cell:target cell interface and promote dephosphorylation of specific intracellular components linked with the activation of NK cell receptors. ITIM-receptor inhibition has been described to suppress degranulation (therefore inhibiting release of perforin and granzymes) and cytokine production (Peterson and Long, 2008).

Activating and inhibitory receptors can be subdivided into three main receptor families: C-type lectin-like receptors, killer immunoglobulin-like receptors, and natural cytotoxicity receptors.

1.2.4.1. C-type lectin-like receptors

C-type lectin-like receptors (CLRs) comprise a large superfamily of receptors, encoded in the natural killer complex, which recognise a diverse range of ligands (Dambuza and Brown, 2015). The terminology of C-type lectin-like receptors derives from C-type lectins. C-type lectins are a group of proteins in which carbohydrate-binding activity, mediated through a carbohydrate recognition domain (CRD), is Ca^{2+}-dependent. Biochemical and functional analyses have shown that, despite having carbohydrate recognition domains, C-type lectin-like receptors cannot bind carbohydrates in a Ca^{2+}-dependent manner; therefore, the conserved motif involved in carbohydrate binding was thus termed C-type lectin-like domain (CTLD) (Drickamer, 1999; Drickamer and Fadden, 2002). CLRs have also been shown to recognize non-carbohydrate ligands, such as lipids and proteins (Zelensky and Gready, 2005).

C-type lectin-like receptors are primarily expressed in myeloid cells such as monocytes, macrophages, neutrophils, and dendritic cells (Dambuza and Brown, 2015). C-type lectin-

like receptors comprise both inhibitory and activating receptors that can signal either directly, through integral signalling motifs, or indirectly, through the association with adaptor proteins (Chiffoleau, 2018). The functions of CLRs in immunity range from host defence against fungi and bacteria, to autoimmunity and tumour cytotoxicity. Growing evidence also indicates involvement of C-type lectin-like receptors in the modulation of adaptive immune responses (Chiffoleau, 2018; Dambuza and Brown, 2015).

C-type lectin-like receptors are typically type II transmembrane glycoproteins with a N-terminal cytoplasmic domain, a transmembrane domain followed by a stalk domain, and an extracellular C-type lectin-like domain at the N-terminus. The CTLD is comprised of two α-helices and two antiparallel β-sheets stabilized by two or three conserved intramolecular disulphide bonds. In addition, CLRs usually dimerized in a homo- or hetero-manner via the cysteine residue present on the stalk region.

Members of the C-type lectin-like family include the NK cell receptors from the CLEC2 family (i.e., human CD69, KACL, AICL, and LLT1, and mouse CLRB), the KLR family (i.e., human NKPR1 and murine Ly49), and the standalone CD94/NKG2x receptors (Bartel et al., 2013).

1.2.4.2. Killer immunoglobulin-like receptors

Killer immunoglobulin-like receptors (KIRs) are a family of transmembrane receptors encoded in the leukocyte receptor complex on human chromosome 19q13.4. The human KIR family is encoded in 14 polymorphic genes. Distinct receptors can transduce either activating or inhibitory signals. KIR classification is based on the number of extracellular immunoglobulin-like domains (D0, D1, and D2 domains) and cytoplasmic tail length (L or S for long or short tails, respectively) (Campbell and Purdy, 2011). The functional activity of KIRs can be predicted by analysing the cytoplasmic tail length and presence of a charged amino acid in the transmembrane region of the molecule. Inhibitory forms of KIRs are, with a few exceptions, long-tailed, whereas KIRs with shorter cytoplasmic tails are activating receptors. Activating receptors possess a charged amino acid in the transmembrane domain necessary for positive signalling upon binding with an ITAM-possessing molecule (MacFarlane and Campbell, 2006).

Killer immunoglobulin-like receptor expression has been reported predominantly on NK cells and to a lesser extent on subpopulations of T lymphocytes. NK cells detect absence or

downregulation of MHC class I molecules by an array of specific complementary systems. Killer immunoglobulin-like receptors preferentially recognize human leukocyte antigen (HLA)-A, -B, -C, and in very specific cases, HLA-G allotypes (Boyton and Altmann, 2007). The highly variable and polymorphic system of KIRs is key in the direct recognition of diverse MHC class I molecules thus pointing to vital roles of KIRs in the regulation of development, tolerance, and activation of NK cells (Campbell and Purdy, 2011; Vilches and Parham, 2002). KIRs have been implicated in immune physiological and pathological mechanisms. Binding of KIRs to their MHC class I ligands on potential target cells results in the modulation of cytotoxicity and cytokine secretion by NK cells. Despite their role in mounting effective responses to infectious diseases and tumours, emerging evidence additionally implicates KIRs in human autoimmune pathogenesis (Bashirova et al., 2006; Lanier, 2005).

1.2.4.3. Natural cytotoxicity receptors

Natural cytotoxicity receptors (NCRs) are a family of immunoglobulin-like receptors encoded in the leukocyte receptor complex. In the 1990s three natural cytotoxicity receptors were first described on human NK cells: NKp46 (NCR1; CD335), NKp44 (NCR2; CD336), and NKp30 (NCR3; CD337). Natural cytotoxicity receptors were initially grouped together due to their ability to activate natural killer cells and kill tumour cells *in vitro* (Pende et al., 1999). Despite functional similarities, the members of the NCR family do not share similarities in amino acid sequence or in structure (Kruse et al., 2014).

NCRs are mostly expressed in NK cells, although recent evidence points to expression in T lymphocytes as well. Natural cytotoxicity receptors are type I membrane proteins comprised by an extracellular ligand-binding domain, a transmembrane domain, and a short cytosolic domain. NCRs lack a functional intracellular signalling domain and therefore must associate with adaptor proteins via a charged residue in their transmembrane domain (Koch et al., 2013). Natural cytotoxicity receptors appear to preferentially recognize and bind pathogen-derived molecules and non-MHC self-molecules unlike other NK cell receptor families that preferentially bind self-MHC and MHC-related ligands (Hudspeth et al., 2013).

NCRs functions in the immune system, although also described for tumour cytotoxicity, are strongly related with NK cell activation in antiviral and pathogen-derived immune responses (Koch et al., 2013). In addition to their cytotoxicity-promoting activities, NCRs can also

mediate the production of proinflammatory cytokines by NK cells thus promoting pathogen clearance and immune response modulation (Hudspeth et al., 2013).

1.3. CD69

Early activation antigen CD69 (also known as C-type lectin domain family 2 member C) is a member of the C-type lectin domain-containing (CLEC) family 2 of natural killer cell receptors (Weis et al., 1998). CD69 is encoded by the CD69 gene located in the natural killer gene cluster on chromosome 12p12-p13 (Renedo et al., 1997; Suto et al., 1997) . CD69 spans approximately 7.5 kb and contains five exons – exons I and II encode the cytoplasmic and transmembrane domains, with the remaining exons encoding for the ectodomain of the protein (Vazquez et al., 2009).

CD69 is constitutively expressed upon activation in all bone marrow-derived cells (e.g., neutrophils, lymphocytes, platelets, and NK cells) with the exception of erythrocytes (Sancho et al., 2005; Testi et al., 1994). Gene expression is detected approximately 30-60 min post activation followed by a rapid decline after 4 to 6 hours. Early transcriptional expression and protein expression (as early as 2-3 h after stimulation) underly the use of CD69 as a very early activation marker of human lymphocytes (López-Cabrera et al., 1993). Constitutive and inducible expression of CD69 is tightly regulated at the transcriptional level due to the almost exclusive expression of the gene in inflammatory sites, thus suggesting a role of inflammatory cytokines in the control of the gene expression (López-Cabrera et al., 1995). Sequence analysis of CD69 revealed the presence of several putative binding sequences for inducible transcription factors (NF-κB, Egr-1, AP-1) that mediate the expression of the gene. Analysis of CD69 promoter showed the presence of three NF-κB motifs that appear to mediate TNF-α-induced expression by the interaction with an array of protein complexes from the NF-κB/Re1 family. Regulation of the gene encoding for CD69 also occurs at the post-translational level by a rapid degradation pathway associated with AU-rich motifs that have been reported in several genes involved in inflammatory and activation responses (López-Cabrera et al., 1995; Santis et al., 1995). An interesting aspect regarding CD69 and proinflammatory cytokine TNF-α is that the cytokine is known to be involved in the expression of the CD69 gene, whilst CD69 receptor has also been reported to induce the synthesis of TNF-α by lymphoid cells, thus establishing a positive feed-back loop between CD69 expression and TNF-α production leading to the maintenance of the inflammatory process (Santis et al., 1992).

1.3.1. Structure of CD69

CD69 is a human type II C-type lectin-like integral transmembrane protein. Human CD69 is a disulphide-linked homodimer with two motifs for extracellular N-glycosylation sites – typical (Asn-X-Ser/Thr) and atypical (Asn-X-Cys) motifs, resulting in subunits of molecular mass ranging from 28 to 32 kDa depending on glycosylation degree (Vance et al., 1997). Early activation marker CD69 is comprised of an extracellular C-terminal protein motif termed C-type lectin-like domain, a stalk region, and an N-terminal cytoplasmic domain (López-Cabrera et al., 1993).

Functional analysis of CD69 domains using CD69/CD23 chimeras by Sancho and colleagues clarified the biological roles associated with each composing domain of the protein. The presence of a Cys68 residue in the N terminal region of CD69 was shown to be responsible for protein dimerization. The transmembrane and cytoplasmic domains are involved in signal transduction by mobilization of extracellular Ca^{2+} stores (Sancho et al., 2000).

To this date five different three-dimensional crystal structures have been resolved for the ectodomain of CD69 – PDB structures 3CCK, 1E87, 1E8I, 1FM5, and 3HUP (Figure 4; page 23). Detailed description of CD69 CTLD showed a consistent structural pattern with other C-type lectin-like receptors, although with some structural differences. CD69 consists of two α-helices and two antiparallel β-sheets. Seven cysteine residues were located; six of which are involved in the formation of intrachain disulphide bonds in the CTLD and the remaining residue involved in homodimer formation. Consistent with previous findings, CD69 possesses only one residue involved in Ca^{2+} coordination required for carbohydrate binding. A putative ligand binding site for CD69 has been proposed by superimposing CD69 backbone structure with Ly49A structure. Residues Asp171 and Glu185 might be available for carbohydrate and MHC class I protein interaction and thus suggesting that these amino acids might be located in the physiological ligand binding site of CD69 (Kolenko et al., 2009; Natarajan et al., 2000).

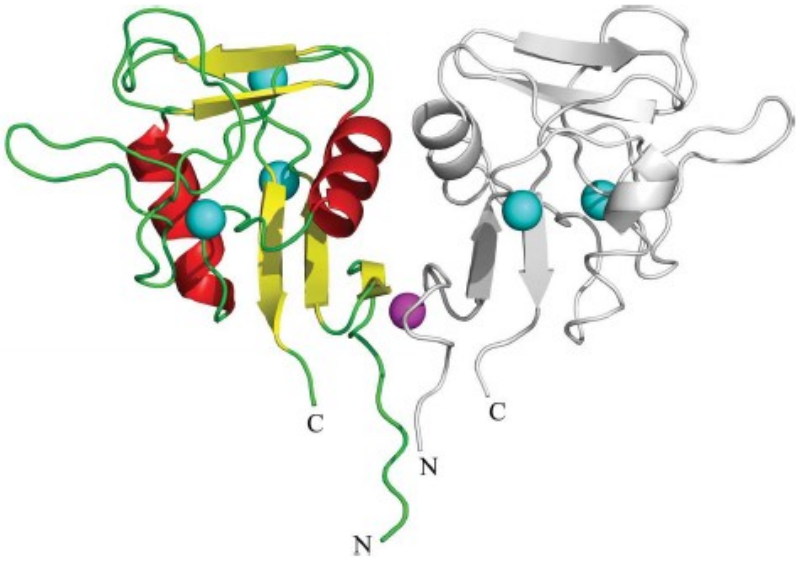

Figure 4 – High-resolution structure of the extracellular domain of homodimeric CD69 represented by coloured secondary-structure elements. Representation of chain A (shown with colours) and chain B (in grey). In chain A, two α-helices (in red) and β-strands (yellow) are shown. Additionally, sodium (magenta) and chloride ions (cyan) are presented. Figure from (Kolenko et al., 2009) (PDB code 3HUP).

1.3.2. Functions of CD69

In addition to the role of CD69 as an activation marker, recent evidence suggests an involvement in regulation of immune responses. Recent identification of putative ligands for CD69 has provided relevant information regarding the functions of the receptor in physiological and pathological circumstances. Functional studies have shown compelling evidence of CD69 as a regulator of lymphocyte migration and retention through its interaction with $S1P_1$. In addition to experimental results in lymphocyte egress regulation and immunomodulation, preliminary information from metabolic studies have shown that CD69 modulates mTOR signalling thus potentially modulating lymphocyte immune responses under specific environmental cues, such as amino acid abundance and hypoxia (Cibrián and Sánchez-Madrid, 2017).

1.3.3. Ligands of CD69

Despite extensive characterization of CD69, the identification of protein ligands was lacking for several decades. In the last years, a number of putative ligands for CD69 have been identified – sphingosine 1-phosphate receptor ($S1P_1$), S100A8/S100A9 complex (also

known as calprotectin), myosin light chains 9 and 12 (Myl9 and Myl12), and Galectin-1. Identification and detailed characterization of protein ligands for CD69 is critical in understanding the role of the NK cell receptor in mechanisms of immunophysiology and immunopathology.

Studies on the generation of functional T cells in the thymus have provided the first evidence in the direct involvement of CD69 in thymocyte development and selection (Feng et al., 2002; Nakayama et al., 2002). Initial findings on the involvement of CD69 in lymphocyte activation and sequestration coincided with the finding that $S1P1_1$, a G-protein-coupled receptor (GPCR), is required within lymphocytes for egress from lymphoid organs; thus pointing to a possible first putative protein ligand for CD69 (Shiow et al., 2006). Lymphocyte egress from lymphoid organs into circulation is essential for normal immune function. The mechanisms that control egress in physiological and pathological conditions are controlled to some extent by a concerted action of CD69 and $S1P_1$. CD69 engagement in GPCR negative regulation, by the formation of a complex with $S1P_1$, promotes downregulation of the receptor thus resulting in egress inhibition, a process thought to improve the ability to mount a local immune response (Bankovich et al., 2010; Cyster and Schwab, 2012; Feng et al., 2002). Despite extensive reports on the functions resulting from CD69:$S1P_1$ interaction, no description of the structure of the complex has yet been reported. Nevertheless, Bankovich and colleagues have mapped the regions of CD69 and $S1P_1$ required for complex formation and receptor downmodulation. In a series of mutagenesis and domain swapping experiments, the authors identified the involvement of the transmembrane and membrane proximal regions of CD69 with helix 4 of $S1P_1$ during complex formation (Bankovich et al., 2010).

The identification of a new putative protein ligand for CD69 was also reported by Lin and colleagues (Lin et al., 2015). Functionals studies, in addition to coimmunoprecipitation and mass spectrometry, described the glycosylation-dependent interaction between CD69 and S100A8/S100A9 complex. S100A8 and S100A9 proteins belong to the S100 protein family; a family characterized by calcium-binding properties and homo- and hetero multimeric formation as a crucial mechanism for appropriate functioning (Leukert et al., 2005). S100A8 and S100A9 proteins are constitutively expressed in granulocytes, monocytes and DCs, and have been reported as having effector functions in immune modulation, as well as in, antimicrobial, oxidant-scavenging, and apoptosis-inducing activities (Stríz and

Trebichavský, 2004). Although a detailed mechanistic understanding of CD69:S100A8/S100A9 complex formation and interaction is lacking, a functional description for the complex has been reported. CD69:S100A8/S100A9 signalling was shown to regulate TGF-β and IL-4 secretion thus promoting regulatory T cell differentiation, in a process dependent on N-glycan moiety presence on the receptor. These observations provide additional experimental evidence in the involvement of CD69 in the regulation of immune homeostasis presumably through ligand-mediated and cell-type-specific signalling (Lin et al., 2015).

Further putative protein ligands for CD69 have been recently proposed. Hayashizaki and colleagues presented the "CD69-Myl9/12 system" where CD69 associates with myosin light chains 9 and 12 in a glycosylation-dependent manner. Functional studies have shown an involvement in the regulation of airway inflammation where Myl9/12 is known to form net-like structures inside blood vessels. These structures appear to promote migration and recruitment of CD69-expressing leukocytes into inflammatory organs (Hayashizaki et al., 2016). Like in the case of CD69:S100A8/S100A9 interaction, no mechanistic description of the CD69:Myl9/12 complex has yet been reported.

Description of lectin Galectin-1, as another putative ligand for early activation antigen CD69, has been provided by de la Fuente and colleagues. The authors demonstrated for the first time the presence of a cell membrane ligand for CD69 on human monocyte-derived dendritic cells. Experimental evidence was provided by biophysical and functional analyses, namely by mass spectrometry, surface plasmon resonance, and binding assays. Interaction of CD69 with galectin-1 was shown to be partially inhibited by lactose, indicating an involvement of the carbohydrate recognition domain in the interaction. Like what has been described for the remaining putative ligands, the interaction also appears to be carbohydrate-dependent. The previously described role of galectin-1 in regulation of Th17 differentiation (Cedeno-Laurent et al., 2010) has been reported to occur through the interaction with CD69, thus supporting the participation of CD69 in immunomodulation in inflammatory conditions (de la Fuente et al., 2014).

1.4. Lectins

Lectins are a superfamily of structurally diverse proteins that preferentially recognize and bind carbohydrate complexes with considerable specificity (Rini, 1995). Lectins are present

in all types of organisms including plants, fungi, bacteria, viruses, and animals (Dodd and Drickamer, 2001).

Lectins were initially described in plants in the end of the 19th century by Hermann Stillmark who reported that seed extracts from the plant *Ricinus communis* contained a protein able to agglutinate animal red blood cells; the protein was thus named by Stillmark ricin. Simultaneously to the description of plant lectins, several other animal lectins were discovered although at the time it was unknown that these proteins were in fact lectins. The first suggestion of animal lectins arose in the beginning of the 1900s in a study of erythrocyte agglutination and lysis by a range of snake venoms (Flexner and Noguchi, 1902; Kilpatrick, 2002).

Animal lectins have been extensively described both structurally and functionally. Lectins are known to play pivotal roles in immune and non-immune processes. Certain animal lectins play roles in quality control and protein trafficking along the lysosomal enzyme secretory pathway (Hauri et al., 2000), whilst others function as recognition molecule within the immune system. Involvement of lectins in immune mechanisms may be subdivided into four types of functions: direct defence; recognition and trafficking within the immune system; immune regulation; and prevention of autoimmunity (Kilpatrick, 2002).

1.4.1. Classification of lectins

The first general classification of lectins derived from the field of plant lectins were the grouping was based on the ability of the protein to recognize and bind certain sequences with varying affinities. Classifications based on amino acid sequence homology and patterns of evolutionary relatedness were proposed in the 1990s with the advent of molecular technologies. The major lectin families include C-type lectins, P-type lectins, I-type lectins, and galectins (previously named S-type lectins) (Figure 5; page 27).

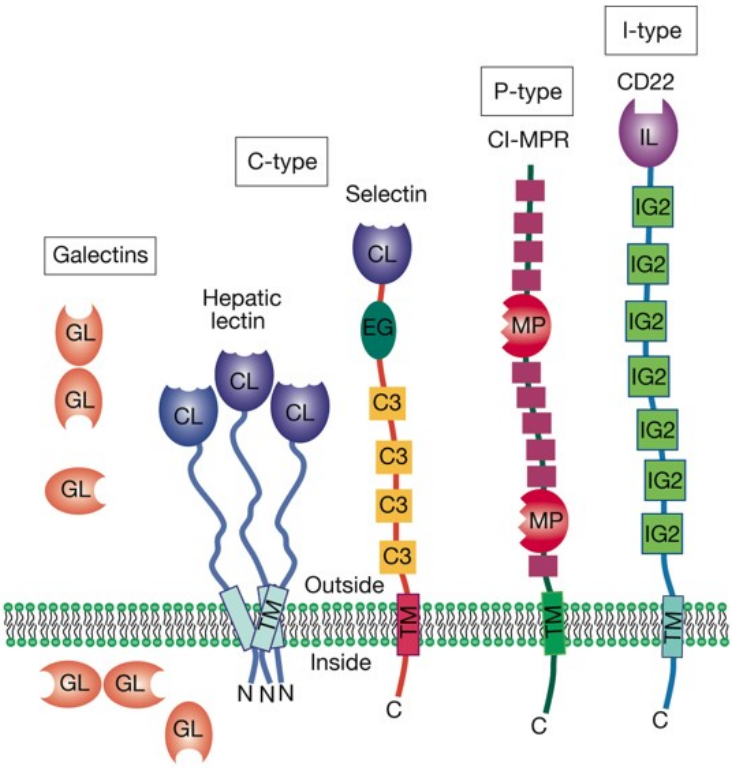

Figure 5 – Schematic representation of major types of animal lectins based on protein structure. The domains that can be found in different lectin families include (CL) C-type lectin CRD, (GL) galectin CRD, (MP) P-type lectin CRD; (IL) I-type lectin CRD, (EG) EGF-like domain, (IG2) immunoglobulin C2-set domain, (C3) complement regulatory repeat, and (TM) transmembrane region (Varki et al., 2009).

1.4.1.1. C-type lectins

The C-type lectin family is the largest family of lectins comprising more than a thousand proteins that recognize a broad range of ligands. C-type lectins are associated with Ca^{2+}-dependent carbohydrate binding through conserved residues (Glu-Pro-Asn for mannose-type specificity, and Gln-Pro-Asp for galactose-type specificity) within the carbohydrate recognition domain. Initial classification of C-type lectins grouped the proteins into seven subfamilies; ten new subfamilies have been recently added to the classification. Examples of subfamilies include tetranectins, attractins, macrophage mannose receptor, selectins, proteoglycans, collectins, type II receptors, free CTLD and NK cell receptors (Zelensky and Gready, 2005). Mammalian C-type lectins exist physiologically either as secreted molecules or as transmembrane proteins, thus explaining the broad range of functions in which this lectin family is involved. Soluble C-type lectins appear to be involved directly in the regulation of development, coagulation, angiogenesis and inflammatory processes whereas

transmembrane C-type lectins appear to modulate cellular, homeostatic and immunological responses.

1.4.1.2. P-type lectins

P-type lectin family is comprised of two members – the cation-dependent mannose 6-phosphate receptor and the insulin-like growth factor II/mannose 6-phosphate receptor. P-type lectins are distinguished from all other lectin families by their ability to recognize and bind phosphorylated mannose residues. Functions associated with P-type lectins include apoptosis, viral entry and transmission between cells, and proteolytic activation of enzyme and growth factor precursors in addition to lysosomal trafficking (Dahms and Hancock, 2002).

1.4.1.3. I-type lectins

I-type lectins form a family consisting of carbohydrate-recognizing proteins that belong to the immunoglobulin superfamily. Additionally, a considerable number of I-type lectins have been described as specifically recognizing and binding to sialic acids; sialic acid-binding immunoglobulin superfamily lectins, also known as Siglecs, comprise the major subclass of I-type lectins (Angata and Brinkman-Van der Linden, 2002). Lectins of this superfamily participate in a plethora in immune functions, ranging from immune cell modulation, modulation of cytokine production, and importantly, in aiding recognition of self- and non-self-molecules thus participating in mechanisms of self-tolerance (Macauley et al., 2014)

1.4.1.4. Galectins

Galectins (previously designated S-type lectins) are a phylogenetically conserved family of lectins characterized by a carbohydrate recognition domain responsible for β-galactoside binding and a shared consensus of amino acid sequence (Camby et al., 2006). The mammalian galectin family currently comprises fifteen members that have been classified into three major groups: prototypical, tandem, or chimera galectins. Classification is based on CRD number and organization. Prototypical galectins contain a single CRD and can exist physiologically as monomers (galectin-5, -7, and -10) or homodimers (galectin-1, -2, -11, -13, -14, and -15). Galectins having two CRDs connected via a short linker peptide fall in the group of tandem galectins (galectin-4, -8, -9, and -12). Galectin-3, the sole member of the

chimera group, has a single CRD and an amino-terminal polypeptide tail rich in proline, glycine, and tyrosine residues, with which it can form oligomeric molecules.

Galectins can be intracellularly located or secreted into the extracellular space (Liu and Rabinovich, 2005). Galectins are synthesized on free ribosomes in the cytoplasm, where there is protein accumulation prior to secretion into the extracellular environment. The members of the galectin family lack any recognizable secretion signalling sequence needed for the initiation of the classical or ER/Golgi-dependent secretory pathway. Nevertheless, galectins can be exported from cells by nonclassical protein export (Cooper and Barondes, 1990).

A plethora of functions have been ascribed to galectins. Interestingly, galectin function appears to be dependent on its cellular location – intracellularly, galectins engage primarily in basic cellular functions, while when present in the extracellular environment, galectins appear to rely on their lectin activity to fulfil their functions. Functional studies have linked galectins with mechanisms of cellular proliferation, chemotaxis, cytokine secretion, apoptosis and cell to cell communication. Further contributions to immunity can also be found through modulation of T cell homeostasis and mediation of T-regulatory cell function (Di Lella et al., 2011).

1.4.2. Galectin-1

Galectin-1 (Gal-1) is a prototypical galectin encoded by the *LSGALS1* gene located on chromosome 22q12. Expression of galectin-1 occurs mostly in lymphoid organs, and in immune-privileged sites (e.g., placenta, testis, and cornea) in physiological and pathological conditions. Human galectin-1 exists as a non-covalent homodimer consisting of subunits of one CRD, responsible for β-galactoside binding. At low concentrations (K_d ~7μM) homodimeric galectin-1 can dissociate into its monomeric form whilst still maintaining carbohydrate-binding (Camby et al., 2006).

The three-dimensional crystal structure of human galectin-1 has been determined at 1.7 Å by López-Lucendo and colleagues (Figure 6; page 30) (López-Lucendo et al., 2004). The overall folding of Gal-1 involves a β-sandwich consisting of two antiparallel β-sheets of five and six strands, with the N and C termini of each subunit positioned at the dimer interface. The CRDs are located at the far ends facing the same surface, which creates a negatively charged cleft in the cavity. The dimer integrity is maintained by noncovalent interactions

between the monomers at the interface, and through a well-conserved hydrophobic core, thus explaining the stability of the dimer in molecular terms (López-Lucendo et al., 2004). The carbohydrate-binding site of dimeric galectin-1 is comprised of highly conserved amino acid residues (His44, Asn46, Arg48, Val58, Asn61, Trp68, Glu71, and Arg73) similarly observed in other members of the galectin family. The interactions between the bound carbohydrate ligand and Gal-1 are formed between His44, Arg48, and Asn46 side-chains with the galactose moiety. Additionally, ionic protein-protein interactions formed by salt bridges in between the residues Arg48, Asp54, Arg73, and Glu71 support the carbohydrate-protein interaction by orienting the side-chains involved in sugar binding to its optimal positions.

Regarding its functions, galectin-1 was initially described as a β-galactoside-binding lectin; it is now clear that despite being able to bind carbohydrates, galectin-1 can also engage in protein-protein interactions. Galectin-1 preferentially binds glycoconjugates containing *N*-acetyllactosamine in multiantenary repeating chains ($K_d \sim 4$ μM); nevertheless, Gal-1 can also interact with individual acetyllactosamine units or with free ligands in solution, although with a considerably lower affinity ($K_d \sim 50$ μM). Besides the function associated with Galectin-1 lectin activity, a plethora of other functions have been described for the protein ranging from modulation of cell growth in cell signalling pathways, to mechanisms of adhesion, motility, and invasion, to main roles in the immune system. Galectin-1 has also been shown to participate directly in mechanisms of initiation, amplification, and resolution of inflammatory processes.

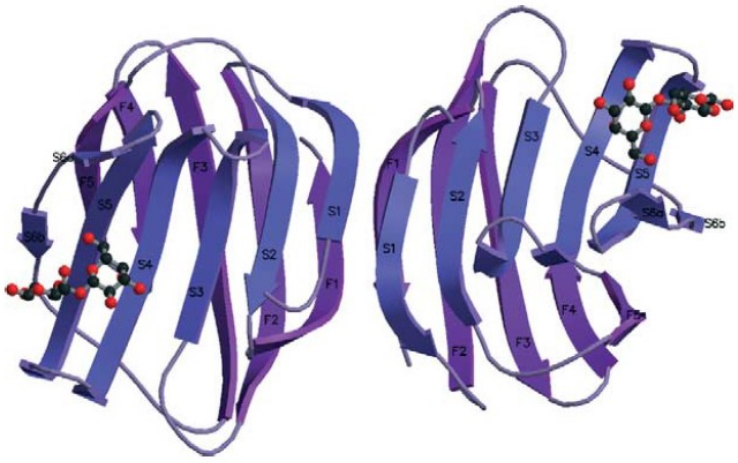

Figure 6 – Three-dimensional X-ray structure of homodimeric human Galectin-1 represented in a ribbon diagram. Representation of Gal-1 fold with a β-sandwich consisting of two antiparallel β-sheets of five (F1-F5) and six (S1-S6a/b) strands, respectively (PDB code 1GZW) (López-Lucendo et al., 2004).

2. Aims of the thesis

- Recombinant expression of cysteine-less mutant of Galectin-1 in *E. coli* BL21(DE3) cells

- Recombinant expression of varying glycoforms of the extracellular domain of CD69 in HEK293 cells

- Purification and characterization of recombinantly expressed proteins

- Study of interaction between NK cell receptors and wild-type or cysteine-less mutant Galectin-1

- Study of N-glycan moiety dependency in interaction between CD69 and wild-type Galectin-1

3. Materials

3.1. Instruments and equipment

Analytical Ultracentrifuge Proteomelab XL-I	Beckman Coulter, USA
Apparatus for SDS-PAGE	Bio-Rad, Germany
Automatic Pipettes	Gilson, USA
Burner	VERKON, Czech Republic
Centrifuge Allegra X-22R	Beckman Coulter, USA
Centrifuge EBA 12R	Hettich, Germany
Centrifuge tubes Oak Ridge	Sigma, USA
Column HiTrap Desalting Sephadex G-25	GE Healthcare, USA
Column HiTrap Talon Crude 5 ml	GE Healthcare, USA
Column Superdex 200 10/300 GL	GE Healthcare, USA
Column Superdex 200 Increase 10/300 GL	GE Healthcare, USA
Concentrator Amicon Ultra (MWCO 10,000)	Millipore, USA
Flow Box BIO 126	LABOX, Czech Republic
Flow Box Clean Air	PMV, Netherlands
HPLC System ÄKTA Basic	GE Healthcare, USA
Incubator CO_2 MC0-18AIC	Sanyo, Japan
Incubator IR 1500	LABsystem, Czech Republic
Laminar box BIO 126	LABOX, Czech Republic
Laminar box Clean Air	PMV, Netherlands
Monolith NT.115	NanoTemper, Germany
Monolith NT.Label Free	NanoTemper, Germany
pH meter Φ	Beckman Coulter, USA
Plastics for cell culture	Sigma, USA
Prometheus NT.48	NanoTemper, Germany
Rotatory Evaporator CentriVap DNA	Labconco, USA
Set for Agarose Gel Electrophoresis	Biokeystone, USA
Shaker Celltron	Infors HT, Switzerland
Shaker Multitron Cell	Infors HT, Switzerland
Spectrophotometer DeNovix DS-11+	DeNovix, USA

Standard capillaries for Monolith NT.115	NanoTemper, Germany
Standard capillaries for Monolith NT.Label Free	NanoTemper, Germany
Standard capillaries for Prometheus NT.48	NanoTemper, Germany
Thermoblock LS1	VLM, Germany
Thermocycler Rotor-Gene 2000	Corbett Life Science, USA
Ultrasound homogenizer Sonoplus	Bandelin, Germany
Vertical electrophoresis apparatus	Bio-Rad, Germany
Vortex Shaker	VELP Scientifica, Italy
Zetasizer Ultra	Malvern Panalytical, UK

3.2. Chemicals

1 kb DNA standard	New England Biolabs, USA
100 bp DNA standard	New England Biolabs, USA
2-mercaptoethanol	Sigma, USA
Acetic acid (CH_3COOH)	Lach-Ner, Czech Republic
Acrylamide	Sigma, USA
Agar	Oxoid, UK
Agarose	Sigma, USA
Ammonium persulfate	Serva, USA
Ampicillin	Biotika, Slovakia
APS	Serva, USA
Bromophenol blue	Lachema, Czech Republic
BSA	New England Biolabs, USA
Buffer for T4 DNA ligase	New England Biolabs, USA
Buffer NEB1	New England Biolabs, USA
Calcium chloride ($CaCl_2$)	Lach-Ner, Czech Republic
Carbenicillin	Biotika, Slovakia
Coomassie Brilliant Blue R-250	Serva, USA
dNTPs	Top-Bio, Czech Republic
EDTA	Jersey Lab Supply, USA
Ethanol	Lach-Ner, Czech Republic

Glycine	Fluka, Switzerland
GoodView II DNA Stain	Ecoli, Slovakia
Hepes	Sigma-Aldrich, USA
IPTG	Sigma-Aldrich, USA
Isopropanol	Lach-Ner, Czech Republic
Lactose	P-lab, Czech Republic
Leupeptin	Sigma-Aldrich, USA
L-glutamine	Sigma-Aldrich, USA
lPEI 25 kDa	Polysciences, USA
Magnesium chloride ($MgCl_2$)	New England Biolabs, USA
Methanol	P-lab, Czech Republic
N,N'-methylene-bis-acrylamide	Sigma-Aldrich, USA
PCR H_2O	Top-Bio, Czech Republic
Pepstatin	Thermo Scientific, USA
Pluronic F-68	NanoTemper, Germany
PMSF	Thermo Scientific, USA
Q5 Buffer	New England Biolabs, USA
RED-tris-NTA 2nd Generation	NanoTemper, Germany
SDS	Jersey Lab Supply, USA
Sodium Azide	Serva, USA
Sodium chloride (NaCl)	P-lab, Czech Republic
Sodium hydrogen phosphate (Na_2HPO_4)	P-lab, Czech Republic
TEMED	Serva, USA
Tris	Sigma-Aldrich, USA
Trypan Blue Stain	Sigma-Aldrich, USA
Tryptone	Oxoid, USA
Tween-20	Sigma-Aldrich, USA
Valproic acid	Sigma-Aldrich, USA
Yeast extract	ImunaPharm, Slovakia

3.3. Enzymes and proteins

Endoglycosidase F1	Expressed by Mgr. Ondřej Skořepa, CU, Czech Republic
Infusion Enzyme with reaction buffer	Biotool, Switzerland
Lysozyme	Sigma-Aldrich, USA
NKp30_HEK293T	Mgr. Ondřej Skořepa, CU, Czech Republic
Q5 DNA Polymerase	New England Biolabs, USA
Restriction endonuclease NcoI	New England Biolabs, USA
Restriction endonuclease PmeI	New England Biolabs, USA
RNAse A	Sigma-Aldrich, USA
T4 DNA Ligase	New England Biolabs, USA
Wild-type Galectin-1	Petr Pachl, Ph.D., IOCB, Czech Republic

3.4. Solutions and media

- **AA:** 30% acrylamide, 1% N,N'-methylene-bis-acrylamide
- **Buffer 1:** 50 mM Tris, 1 M NaCl, 10 mM $CaCl_2$, 10 mM NaN_3, pH 8,0
- **Buffer 2:** 50 mM Tris, 200 mM NaCl, 10 mM $CaCl_2$, 200 mM lactose, 10 mM NaN_3, pH 8,0
- **Buffer 4:** 50 mM Tris, 200 mM NaCl, 10 mM EDTA, 10 mM NaN_3, pH 8,0
- **Destaining solution for SDS-PAGE:** 35% ethanol, 10% acetic acid
- **Electrode buffer:** 25 mM Tris, 190 mM glycine, 0.1% (w/v) SDS, pH 8,3
- **EX-CELL 293:** Commercially available medium (Sigma-Aldrich, USA) supplemented with L-glutamine to the final concentration of 4 mM
- **HEPES buffer:** 10 mM HEPES, 150 mM NaCl, 10 mM NaN_3, pH 7,5
- **LB medium:** 1% tryptone, 0.5% yeast extract, 1% NaCl, pH 7,4
- **LB agar:** 1.5% agar in LB medium
- **MES buffer:** 20 mM MES, 100 mM NaCl, 10 mM NaN_3, pH 5,0
- **PBS buffer:** 50 mM Na_2HPO_4, 300 mM NaCl, 10 mM NaN_3, pH 7,0

- **PBS buffer with imidazole:** 50 mM Na_2HPO_4, 300 mM NaCl, 10 mM NaN_3, 250 mM imidazole, pH 7,0
- **Staining solution for SDS-PAGE:** 45% methanol, 10% acetic acid, 0.25% CBB R-250
- **TES buffer:** 10 mM Tris, 0,5 mM EDTA, pH 8,0

3.5. Bacterial strains and cell lines

Escherichia coli BL21(DE3)	Thermo Scientific, USA
Escherichia coli DH5α	Thermo Scientific, USA
HEK293S GnTI$^-$	CRL-3022, ATCC, USA
HEK293T	A. Radu Aricescu, UK

3.6. DNA

3.6.1. Vectors

pOPINE_SEC_GAL_STOP

3.6.2. Oligonucleotides for PCR

GAL_E_FW

5’ AGGAGATATACCATGGCTTCTGGTCTGGTCGC 3’

GAL_STOP_E_REV

5’ GTGATGGTGATGTTTTTAGTCAAAGGCCACAGATTTGATCTTG 3’

3.7. Commercial kits and documentation

Monolith His-Tag labelling kit RED-tris-NTA 2nd Generation	NanoTemper, Germany
Monolith NT.115 manual	NanoTemper, Germany
NucleoBond Xtra Midi/Maxi	Macherey-Nagel, Germany
NucleoSpin gel and PCR clean-up	Macherey-Nagel, Germany
NucleoSpin Plasmid	Macherey-Nagel, Germany
Prometheus NT.48 manual	NanoTemper, Germany

4. Methods

4.1. Molecular cloning and DNA manipulation

4.1.1. Polymerase Chain Reaction

DNA of interest was amplified by the polymerase chain reaction (PCR). The PCR reaction was prepared by adding 100 ng of template DNA, 2 µl of forward primer, 2 µl of reverse primer (final concentration of primers was 500 nM), 0.5 µl of 10 mM deoxyribonucleotides (dNTPs), 4 µl of 5 × Q5 buffer, 4 µl of 5 × Q5 polymerase enhancer, and 0.5 µl or 0.4 U of Q5 polymerase. ddH_2O was added to the final volume of 20 µl. Following sample preparation, the 200 µl PCR tubes were briefly centrifuged using a benchtop centrifuge. The prepared PCR reactions were then placed in a thermal cycler programmed with the following steps:

A. 5 min – 95ºC
B. 30 cycles: 30 s – 95ºC; 30 s – 65ºC; 1 min – 72ºC
C. 8 min – 72ºC

After finalizing the program, the temperature in the thermal cycler was decreased to 4ºC.

4.1.2. Preparation of insert and linearized vector

The plasmid was linearized by restriction enzyme cleavage. The restriction reaction was prepared by adding 3 µg of plasmid, 2 µl of 10 × concentrated BSA solution, 2 µl of NEB1 buffer, 1 µl of PmeI and 1 µl of NcoI restriction endonucleases (10 U of each enzyme), and ddH_2O to the final volume of 20 µl. The reaction mix was incubated at 37ºC for 1h. After incubation, the restricted plasmid was analysed by agarose gel electrophoresis.

4.1.3. Agarose gel electrophoresis

Agarose gel electrophoresis was used for isolation and analysis of PCR products or restricted vectors. The agarose gel was prepared by dissolving 0.65 g of agarose in 65 ml of TAE buffer in the microwave for 40 to 60 seconds. After the solution cooled down to approximately 50ºC, 3 µl of GoodView Nucleic Acid Stain were added. The solution was gently mixed, poured in the previously prepared electrophoresis apparatus, the comb was placed into the comb slot and let solidify for approximately 30 minutes. Prior to sample

loading, deionized water was poured on the gel top and the comb removed. TAE buffer was then poured into the positive and negative reservoirs.

The samples were prepared for loading by adding one tenth of 10 × concentrated DNA loading buffer to each sample. The samples were prepared to the final volume of 15 µl. Additionally, 5 µl of 1 kb and 5 µl of 100 bp markers were loaded into the first wells. The gel was then run at 180 V for approximately 30 to 45 minutes. After completion of the electrophoresis, the gel was visualized under UV radiation with wavelength of 312 nm or blue light.

4.1.4. DNA extraction from agarose gel

DNA was extracted from the agarose gel using the PCR clean-up, Gel extraction commercial kit provided by Macherey-Nagel, Germany. The extraction protocol was followed according to the manual provided by the manufacturer.

The gel portion containing the DNA fragment with the expected size was excised from the agarose gel. The weight of the gel portion was then determined, followed by its transfer to a clean tube. 200 µl of buffer NTI were added to 100 mg of agarose gel and incubated at 50ºC for 5-10 min in the thermoblock. The sample was gently mixed every 2-3 min until the gel was completely dissolved. The dissolved sample was then pipetted into a NucleoSpin PCR Clean-up Column previously placed in a collection tube. The sample was centrifuged at 11,000 × g for 30 s and the flow through was discarded. The column was washed by adding 600 µl of buffer NT3 followed by centrifugation at 11,000 × g for 30 s. The flow-through was discarded and the column placed back into the collection tube. The previous step was repeated once again. The column was dried by centrifuging the column at 11,000 × g for 1 min, so that buffer NT3 was completely removed. The final step in the protocol was the elution of DNA, which started by placing the NucleoSpin column into a new 1.5 ml microcentrifuge tube. Plasmid DNA was eluted with the addition of 15-30 µl of elution buffer, previously heated to 70ºC followed incubation at room temperature for 1 min and centrifugation at 11,000 × g for 1 min.

4.1.5. Measurement of DNA concentration and purity

DNA concentration and purity were measured by UV light absorption using DeNovix Ds-11 spectrophotometer. The DNA concentration was determined by pipetting 2 µl of the

sample onto the sample surface and measuring the absorbance at 260 nm. Similarly, the purity was determined by measuring the absorbance at 260 and 280 nm, and its value calculated from the A_{260nm}/A_{280nm} ratio. Before all the measurements, the spectrophotometer was blanked with the buffer used for DNA elution.

4.1.6. Ligation reaction

The ligation mixture was prepared by mixing 100 ng of the plasmid pOPINE and 200 ng of the DNA insert with 0.5 µl of Infusion enzyme, 2 µl of Infusion buffer and dH_2O to the final volume of 10 µl. The reaction mix was briefly centrifuged using a bench microcentrifuge and incubated at 37ºC for 30 min.

4.1.7. Transformation

Prior to transformation, competent *E. coli* DH5α cells were thawed on ice for approximately 30 min. 100 ng – 1 µg of the plasmid with the gene of interest was added to 50 µl of competent cells and gently mixed by flicking. The mixture was incubated on ice for 30 minutes, followed by heat shock at 42°C for 45 sec and 2 min on ice. Afterwards, 1 ml of LB medium preheated at 37 °C was added to the transformation. The samples were then incubated at 37ºC in a shaking incubator for 60 min. The transformed cells were then centrifuged for 3 min at 2000 × g and the majority of the supernatant was discarded. With the remaining supernatant, the cell pellet was resuspended and plated into a previously heated LB agar plate containing 100 µg/ml ampicillin. The plate was incubated overnight (or approximately 16 hours) at 37ºC. The following day, the plates containing colonies were stored at 4ºC until further use.

4.1.8. Colony PCR

In aseptic conditions, bacterial colonies were randomly selected from the agar plates using a 20 µl tip and resuspended in 6 µl of sterile dH_2O in 200 µl sterile PCR tubes. To each tube, 10 µl of Master Mix, 2 µl of reverse primer, and 2 µl of forward primer were added. The final volume of 20 µl was reached by the addition of dH_2O. The tubes were then placed in a thermal cycler with the program:

D. 5 min – 95ºC
E. 20 cycles: 30 s – 95ºC; 30 s – 62ºC; 1 min – 72ºC
F. 10 min – 72ºC

After finalizing the program, the temperature in the thermal cycler was decreased to 4ºC. The PCR products were analysed by agarose gel electrophoresis

4.1.9. Small scale isolation of plasmid DNA

The 20 µl tip used for picking the selected colony for colony PCR was additionally used inoculate 5 ml of sterile LB medium containing 100 µg/ml of ampicillin in 50 ml Falcon tube. Prior to incubation, the cap of the tube was slightly loosen so as to allow proper gas exchange between the bacteria and surrounding environment. Bacteria were then grown at 37ºC and 220 rpm overnight. The following day, plasmid DNA was isolated using the commercially available NucleoSpin Plasmid kit (Macherey-Nagel, Germany). The isolation protocol was followed according to the documentation provided by the manufacturer. Subsequent to incubation, the cell suspension was centrifuged at 3900 × g for 5 min and the resulting supernatant discarded. The pellet was resuspended in 250 µl Buffer A1 by vortexing or pipetting up-and-down several times. 250 µl of Buffer A2 were then added to the resuspended cells and the tubes gently inverted 6-8 times to guarantee a complete mixture. A 5 min incubation at room temperature followed the previous step. Subsequent to incubation, 300 µl of Buffer A3 were added and the components thoroughly mixed by inversion of the tube until the colour changed from blue to colourless. After complete neutralization, the cells were centrifuged at 11,000 × g for 5 min at room temperature; the step was repeated in case the supernatant was not completely clear. The supernatant was transferred to a NucleoSpin column placed in a collection tube and then centrifuged for 1 min at 11,000 × g. The flowthrough was discarded and the column placed back in the collection tube. The column membrane was then washed by adding 500 µl of AW buffer followed by centrifugation at 11,000 × g for 1 min. An additional washing step took place in which 600 µl of Buffer A4, previously supplemented with ethanol, was added to the column. The tube containing the column was incubated at room temperature for 2 min and once again centrifuged at 11,000 × g for 1 min. The flowthrough was discarded and the dry column transferred into a clean Eppendorf tube. The DNA was eluted by incubation of the column at room temperature for 1 min with 50 µl of AE buffer previously heated at 70ºC followed by centrifugation at 11,000 × g for 1 min.

4.1.10. DNA Sequencing

Sequencing of plasmid DNA was performed by the DNA Sequencing Laboratory from the Centre of Service Laboratories of the Faculty of Science, Charles University.

The samples were prepared in 200 µl PCR tubes, into which 200 – 250 ng of DNA and 1 µl of forward or reverse primer were pipetted. The total reaction volume of 8 µl was achieved by the addition of PCR-grade water.

4.1.11. Large scale isolation of plasmid DNA

Competent *E. coli* DH5α cells were transformed with the plasmid DNA and plated into agar Petri dishes as previously described in 4.1.6. In a laminar flow box, 500 ml of sterile LB medium and 500 µl of ampicillin (100 µg/ml) were transferred to a 2 L Erlenmeyer flask. Approximately 5 ml of LB medium was pipetted into the Petri dish and the colonies were thus resuspended using a glass spreader, previously sterilized in the flame. The 5 ml containing the resuspended bacteria were then pipetted into the Erlenmeyer flask containing LB medium and ampicillin. The bacteria were grown in a flask shaking incubator overnight at 37ºC and 220 rpm. After approximately 16 hours, the bacteria were harvested by centrifugation at 3900 × g for 50 min at 4ºC. The resulting supernatant was discarded, the pellet resuspended with 20 ml of TES buffer with the aid of a vortex mixer and centrifuged at 3900 × g for 15 minutes.

Plasmid DNA was isolated using the NucleoBond Xtra Midi/Maxi commercial kit provided by Macherey-Nagel, Germany. The isolation protocol was followed according to the manual provided by the manufacturer. The bacterial pellet was resuspended in 18 ml of RES buffer previously supplemented with 60 µg/ml RNAse A by vortexing. 18 ml of Lysis Buffer LYS were subsequently added to the suspension and gently mixed by inverting the tube 5 times. In the meantime, the NucleoBond Xtra column was equilibrated with 25 ml of Equilibration Buffer EQU. 18 ml of neutralization NEU buffer were added to the suspension and gently mixed by inverting the tubes 5 times. Prior to loading the column with the suspension, the tubes were centrifuged at 20,000 × g for 20 min and the supernatant was loaded into the previously equilibrated NucleoBond Xtra column. Subsequent to column emptying by gravity flow, the column was washed with 25 ml of Wash Buffer and the DNA eluted by 15 ml of Elution Buffer ELU. 10.5 ml of -20 ºC isopropanol were added to precipitate the eluted plasmid DNA, and the mixture was centrifuged at 20,000 × g for 30 min at 4ºC. The

supernatant was discarded, the pellet washed by the addition of 5 ml of -20 ºC 70% (v/v) ethanol, and subsequently centrifuged at 20,000 × g for 10 min at 4ºC. The supernatant was carefully removed, and the DNA pellet dried in a rotary evaporator. The dried DNA pellet was lastly resuspended in 1 ml ddH_2O. DNA concentration and purity were measured following the protocol described in 4.1.5 (page 38).

4.2. Recombinant expression of CSGal-1 in bacterial expression system

Escherichia coli BL21 (DE3) was used for the recombinant expression of the His-tag-less and cysteine-less mutant of Galectin-1 (CSGal-1).

4.2.1. Recombinant CSGal-1 expression

Competent *E. coli* BL32 (DE3) cells were transformed with the plasmid containing the gene of interest following the heat-shock protocol for bacterial transformation. The transformed cells were plated into a LB agar plate containing 100 µl/ml ampicillin and incubated overnight at 37ºC.

After incubation, one colony from the LB agar plate was randomly selected and used for the preparation of a starter culture. The picked colony was incubated with 5 ml LB medium and 5 µl carbenicillin in a 50 ml Falcon tube overnight at 37ºC and rotational speed of 220 rpm.

The following day, 500 µl of the cell starter culture was transferred to a 2 L Erlenmeyer flask containing 500 ml of LB medium and 500 µl of carbenicillin and incubated at 37ºC and 200 rpm until the optical density at 550 nm reached absorbance values between 0.4 and 0.8. The optical density was tracked by measuring the absorbance at 550 nm in 2-hour intervals. After reaching the optimal OD, the cells were induced with 250 µl of IPTG and incubated overnight at 20ºC and 200 rpm.

4.2.2. Purification of CSGal-1

4.2.2.1. Harvesting

E. coli BL21(DE3) cell cultures were harvested by centrifugation at 3900 × g for 30 minutes. The obtained supernatant was discarded. The pellet was resuspended in 20 ml of TES buffer and centrifuged at 3900 × g for 15 minutes. The obtained supernatant was discarded, and the pellet further processed or immediately stored at -20°C.

4.2.2.2. Lactose-Sepharose affinity chromatography

Prior to the beginning of the purification steps the pellet was thawed on ice. The pellet was then resuspended with Buffer 1 to a final volume of 40 ml. Subsequent to pellet resuspension, 400 µl of PMSF (100 mM), 40 µl of leupeptin (1 µg/ml), 40 µl of pepstatin (1 µg/ml), 40 µl of RNAse (1 µg/ml), and 2 µl of $MgCl_2$ (100 mM) were added and thoroughly mixed. The resuspended pellet was then incubated on ice for 15 minutes. The cell suspension was sonicated with 5 bursts of 60 sec followed by 60 sec of cooling on ice. The suspension was centrifuged at 4ºC for 30 min at 3900 × g. The obtained supernatant was filtered through a 0.22 µm filter and diluted with Buffer 1 to the final volume of 200 ml.

5 ml of Lactose-Sepharose Fast Flow resins (Galab Technologies, Germany) were packed into a chromatography column. Affinity chromatography was performed on HPLC system ÄKTA Basic. The column was equilibrated with 5 column volumes of Buffer 1 or until an equilibrium of UV absorption and conductivity was reached. Following column equilibration, the supernatant was loaded onto the column and the flow through was collected. After medium loading, the column was washed with Buffer 1 until an equilibrium between UV absorption and conductivity was reached again. The protein was isocratically eluted by the loading of Buffer 2. The concentration of the fractions was measured as described in 4.4.1 (page 47). The obtained protein fractions were stored at 4°C until further use.

4.2.2.3. Protein concentrating

The eluted protein fractions were concentrated by using Amicon Ultra (MWCO 10,000) concentrators. The concentrators were filled with protein solution and centrifuged at 3900 × g until the final volume was approximately 250 µl. The concentrated protein was then centrifuged in a clean tube for 6 minutes at 20,000 × g.

4.2.2.4. Lactose removal by size-exclusion chromatography

The concentrated protein was further purified and prepared for binding assays by size-exclusion chromatography. Size-exclusion chromatography was performed on HPLC system ÄKTA Basic with Superdex 200 10/300 GL column. The column was equilibrated with Buffer 4 or until an equilibrium of UV absorption and conductivity was reached. Prior to injection of the sample, the injection loop was washed with 5 ml of Buffer 4. The

concentrated protein was injected onto the column and separated on the column. The eluate was collected by an automated sample collector in 1 ml fractions. The concentration of the fractions was measured as described in 4.4.1 (page 47). The obtained protein fractions were stored at 4°C until further use.

4.2.2.5. Protein recharging by size-exclusion chromatography

The protein was initially concentrated as described in 4.2.2.3 (page 43). The protein recharging was performed on HPLC system ÄKTA Basic with two HiTrap desalting columns. The column was equilibrated with 5 column volumes of Hepes buffer supplemented with 10 mM $CaCl_2$. Prior to injection of the sample, the injection loop was washed with 5 ml of equilibration buffer. The concentrated protein was then injected onto the columns and eluted into Hepes buffer with 10 mM $CaCl_2$. The eluted samples were collected by an automated sample collector in 1 ml fractions. The obtained samples were then concentrated, and the final protein concentration measured as described in 4.2.2.3 (page 43) and 4.4.1 (page 47), respectively. The obtained protein was stored at 4°C until further use.

4.3. Recombinant expression of NK cell receptor domains in mammalian expression system

Recombinant protein expression in HEK293 cell lines was used to express NK cell receptors (i.e., CD69, LLT1, rCLRB, KACL). HEK293S GnTI$^-$ cell line was used to express CD69 with homogenous $Man_5GlcNac_2$ glycosylation, whilst HEK293T cell line was used to express NK cell receptors with wild-type glycosylation.

4.3.1. Recombinant Protein Expression in HEK293 cell line

4.3.1.1. Cultivation of HEK293 cells

HEK293 cells were cultivated in square shaped glass cell culture bottles with gas-permeable membrane screw caps in Celltron shaker at 37ºC, 135 rpm and an atmosphere composed of 5% CO_2. The optimal volume to maintain proper aeration of the cells was 30-40% of total bottle volume.

HEK293 cells were cultivated with the commercial EXCELL293 medium. Twice per week the cells were subcultivated after control of cell density and viability. Part of the cell

resuspension was supplemented with fresh culture medium previously tempered at 37ºC to maintain a resulting cell density of $0.2.10^6$ per ml. The volume of original suspension represented in maximum one tenth of the final volume. In case the resulting volume exceeded 10% of the final volume, the cell suspension was centrifuged at for 5 min at 95 × g and 25ºC and subsequently resuspended in an appropriate volume of culture medium.

4.3.1.2. Cell density counting

To estimate the cell density, 20 µl of cell suspension were pipetted into a sterile 1.5 ml microtube in sterile conditions. 160 µl of a 0.4% trypan blue solution in PBS-TK were added to the 1.5 ml microtube and gently mixed. After a short incubation, 20 µl were pipetted into a haemocytometer for manual counting. Assessment of cell number and viability was performed under the microscope by separately counting the number of dead cells (stained blue) and living cells (transparent) in all nine squares. The total number of living cells was multiplied by 10^4 to yield the cell density in the units of 10^6 per ml. The cell viability was determined by calculating the percentage of living cells in the sum of all cells counted.

4.3.1.3. Transient transfection

Prior to transient transfection, a DNA solution was prepared in PBS-TK buffer. The transfection solution contained 88% expression plasmid, 10% pTW5sec_P27, and 2% pTW5sec_aFGF (cell cycle regulatory proteins). A total of 800 µg of DNA (1 µg per 1 million cells) was diluted in 6 ml of PBS-TK buffer.

Subsequent to the preparation of the transfection solution, the cells were prepared for the transfection by transferring a volume containing 800 million cells into a sterile 50 ml Falcon tube. The cells were centrifuged for 5 min at 95 × g and the resulting supernatant was discarded. The cell pellet was resuspended in 34 ml of EXCELL293 medium, that had been previously tempered at 37ºC, and transferred into a glass cell culture bottle. The DNA transfection mix was filtered through a 0.22 µm filter into the glass bottle containing the resuspended cells. Subsequently, linear polyethylenimine was pipetted into the suspension such that the DNA:lPEI weight ratio was 1:4 (in case of HEK293T) or 1:5 (in case of HEK293S GnTI$^-$). Cells were incubated for 4 hours in the Multitron cell shaker at 37ºC, 135 rpm and 5% CO_2 atmosphere. After the incubation period, 1.6 ml of 0.5 M valproic acid and antibiotics were added to the cells and the total volume made up to 400 ml with EXCELL293 cell culture medium. The cells were harvested 5-7 days later.

4.3.2. Purification of His-tagged proteins

4.3.2.1. Harvesting of HEK293 medium

HEK293 transfections were harvested by centrifugation at 3900 × g for 30 minutes. The obtained pellet was discarded, and the supernatant filtered and diluted with PBS buffer in 1:1 ratio.

4.3.2.2. Immobilized Metal Affinity Chromatography

Immobilized metal affinity chromatography was performed on HPLC system ÄKTA Basic with a HiTrap TALON crude 5 ml column. The column was first equilibrated with 5 volumes of PBS buffer or until equilibrium between conductivity and UV absorption was reached. After the column was equilibrated with PBS buffer, the supernatant was loaded into the column and the flow through was collected. Subsequent to medium loading, the column was washed with PBS buffer to elute unbound proteins. The protein was eluted in a stepwise manner by addition of elution buffer (50 mM Na_2HPO_4, 300 mM NaCl, 10 mM NaN_3, 250 mM imidazole, pH 7,0). The eluate was collected by an automated sample collector in 1 ml fractions. The HiTrap TALON crude column was then regenerated with MES buffer, and sequentially washed with dH_2O, PBS buffer and dH_20. The column was stored in EtOH at 4ºC until further use.

The concentration of the eluted fractions was measured as described in 4.4.1 (page 47) and the samples stored at 4ºC until further use.

4.3.2.3. Size-exclusion chromatography

Prior to size-exclusion chromatography, the protein was concentrated as described in 4.2.2.3 (page 43). Size-exclusion chromatography was performed on HPLC system ÄKTA Basic with Superdex 200 10/300 GL column. The column was equilibrated with Hepes buffer. Prior to injection of the sample, the injection loop was washed with 5 ml of Hepes buffer. The concentrated protein was injected and separated on the column. The eluate was collected by an automated sample collector in 1 ml fractions. The concentration of the fractions was measured as described in 4.4.1 (page 47). The obtained protein fractions were stored at 4°C until further use.

4.4. Protein characterization and preparation for binding assays

4.4.1. Determination of protein concentration

Protein concentration was measured by UV light absorption at 280 nm using DS-11 FX+ spectrophotometer and calculated based on molecular weight and predicted extinction coefficient. Protein parameters were calculated from the amino acid sequences into ExPASy ProtParam tool (Gasteiger et al., 2005). All the measurements were blanked with the solvent of the samples.

4.4.2. SDS-PAGE

Obtained protein samples were resolved and analysed by SDS-PAGE. The standard SDS-PAGE setup involves the use of the discontinuous Laemmli buffer system, in which the gel and electrode reservoirs have different buffers.

SDS-PAGE started by the running gel preparation, followed by preparation of the stacking gel. The running gel (15% of acrylamide) was prepared by adding 0.9 ml of H_2O, 1 ml of 1M Tris-HCl pH 8.8, and 40 µl SDS. 2 µl of TEMED and 40 µl were added lastly to previously prepared solution. The solution was gently mixed, pipetted into the previously assembled gel-casting sandwich and overlaid with deionized water to prevent polymerization inhibition by oxygen. While the running gel was polymerizing (approximately 30 min), the stacking gel was prepared by mixing 0.7 ml of ddH_2O, 0.125 ml of 1M Tris-HCl pH 6.8, 10 µl SDS, and at last, 1.5 µl of TEMED and 10 µl of APS. The water overlaying the running gel was removed, the stacking solution gently mixed, pipetted on top of the running gel and the comb placed onto the gel. After polymerization, the gel-casting sandwich was placed in the electrophoresis chamber, running buffer added to the gel reservoir and the comb removed.

Samples for SDS-PAGE were prepared in both reducing and non-reducing conditions. For each sample, 5 to 10 µg of protein were pipetted into a 1.5 ml microtube to which 3 µl of 5x concentrated sample buffer (reducing or non-reducing) were added. dH_2O was added to reach the final sample volume of 15 µl and the samples shortly centrifuged in benchtop centrifuge. The samples were boiled at 95ºC for 5 minutes, followed by a short centrifugation and loading into the wells of the prepared gel. In addition to the samples to be resolved, 3 µl of molecular weight ladder was loaded into the first gel lane.

SDS-PAGE ran at 200 V for 40 – 55 minutes. After the end of the electrophoretic separation, the gels were stained overnight with a staining solution for SDS-PAGE. The following day, the gels were destained by adding a destaining solution for SDS-PAGE; this step was repeated several times until the gels were sufficiently destained. The gels were digitalized by scanning and stored in ethanol until further use.

4.4.3. Protein deglycosylation

NK cell receptors were enzymatically deglycosylated in order to study the N-glycan moiety dependency in the interaction with galectin-1. NK cell receptors, namely CD69_CM1 and CD69_C2 expressed in HEK293S GnTI$^-$ cell line, were enzymatically deglycosylated by mixing 0,5 mg of protein with 10x C5 reaction buffer (1:10 ratio) and with 10 µl of 1 mg/ml endoglycosidase F1. The samples were incubated at 37ºC for 4h, followed by incubation overnight at room temperature, and storage at 4ºC until further use. Prior to purification by size-exclusion chromatography, the samples were centrifuged at 25,000 × g for 6 min. The samples were then purified by size-exclusion chromatography as described in 4.3.2.4.

4.4.4. Nano Differential Scanning Fluorimetry

Nano differential scanning fluorimetry (nanoDSF) was performed using Prometheus NT.48 (NanoTemper, Germany) in the Centre of Molecular Structure in BIOCEV with the technical support by Tatsiana Charnavets, Ph.D.

Prior to the measurements, the samples were centrifuged for 10 min at 10,000 × g. The samples were measured in the temperature range from 20 ºC to 95 ºC with incremental increases in temperature of 1.5 ºC per minute. The data was collected and analysed using the software programs PT.ThermControl and PR.Stability analysis, respectively.

4.4.5. Dynamic Light Scattering

Dynamic light scattering (DLS) was measured using Zetasizer Ultra (Malvern Panalytical, UK) in the Centre of Molecular Structure in BIOCEV with the technical support by Tatsiana Charnavets, Ph.D.

Prior to the measurements, the samples were centrifuged for 10 min at 10,000 × g. After centrifugation, 40 µl of 1 mg/ml protein sample were pipetted into an ultra-low volume ZEN2112 quartz cuvette (Malvern Panalytical, UK). For each measurement the following method was used: four measurements of protein size followed by one measurement of multi-

angle dynamic light scattering at 25ºC with an equilibration time of 120 s and a return to default temperature in between each measurement. The data was collected and processed using the General Purpose analysis model provided by the ZS Xplorer Software (Malvern Panalytical, *UK*).

4.4.6. Analytical Ultracentrifugation

Analytical ultracentrifugation was performed by RNDr. Ondřej Vaněk, Ph.D., at the Department of Biochemistry, Faculty of Science, Charles University, using analytical ultracentrifuge ProteomeLab XL-I and sedimentation velocity experiment.

Analytical ultracentrifugation was performed to analyse the sedimentation velocities of wtGal-1 and CSGal-1. For each experiment 60 μM of protein were measured. Analysis was performed at 48,000 rpm and 20ºC using An50-Ti rotor. 200 absorbance scans were taken in 4 min intervals at 280 nm wavelength. Hepes buffer was used as a reference. The buffer density and viscosity, and partial specific volume of analysed proteins were predicted by SEDNTERP software (Laue et al., 1992) and the data analysed by SEDFIT software (Schuck, 2000).

4.4.7. Label-free Microscale Thermophoresis

The lectin activity of the recombinantly expressed CSGal-1 was assessed by label-free Microscale Thermophoresis (label-free MST) using Monolith NT.LabelFree in the Centre of Molecular Structure in BIOCEV with the technical support by Mgr. Tomáš Kovaľ, Ph.D. and Tatsiana Charnavets, Ph.D.

Before the preparation of the samples, all the protein solutions and buffers were centrifuged at 10,000 × g for 10 min at 4ºC to precipitate any impurify in the form of a pellet. The supernatant was transferred into a clean Eppendorf microtube and the pellet was discarded. For each measurement, 16 sterile PCR tubes were used. By reverse pipetting, 10 μl of Hepes supplemented with 0.1% pluronic F-127 were transferred to tubes 2-16. 10 μl of 5 mM lactose solution in Hepes were then pipetted to tubes 1 and 2. The samples on tube 2 were mixed by pipetting up-and-down multiple times. From tube 2, 10 μl were transferred to tube 3 and mixed by pipetting up-and-down several times to ensure a proper dilution. The step was repeated for tubes 4-16, with 10 μl of solution being removed from tube 16 in the end (Figure 7; page 50).

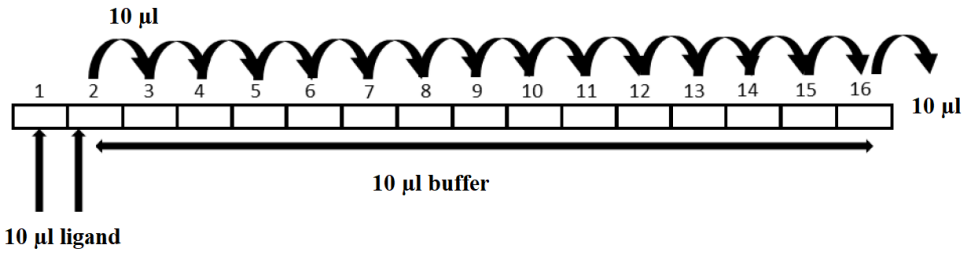

Figure 7 – Schematic representation of MST sample preparation. Adapted from (Duhr and Braun, 2006).

The samples were briefly centrifuged to ensure that all the volume was at the bottom of the tubes. 10 µl of 1 µM CSGal-1 were pipetted to each of the 16 PCR tubes followed by centrifugation at 10,000 × g for 10 min at 4ºC.

After centrifugation the samples were loaded into Standard Monolith NT.LabelFree Capillaries (NanoTemper, Germany) and the measurements initiated. The initial measurement consisted of a pre-test to assess the intrinsic fluorescence of all the components used in the experiment (i.e., buffer, ligand, and target protein). The CSGal-1:lactose interaction was measured at 20% MST power and 80% LED power with the time settings 5 s fluorescence before, 30 s MST on, 5 s fluorescence after, and 25 s delay. For statistical significance, the samples were prepared and measured in triplicates in an independent manner. The data was collected by NT.Control Software and analysed by MO.Affinity analysis using expert mode.

4.5. Validation of binding

4.5.1. Microscale Thermophoresis

Microscale thermophoresis was initially employed to assess the binding between NK cell receptors and galectin-1, and later to the study of N-glycan moiety dependency in the protein:protein interactions. MST was measured using Monolith NT.115 in the Centre of Molecular Structure in BIOCEV with the aid of Mgr. Tomáš Kovaľ, Ph.D.

Prior to measurements, all the samples were centrifuged using a benchtop centrifuge for 10 min at 10,000 × g. His-tagged proteins were labelled with Monolith His-tag labelling kit RED-tris-NTA 2nd Generation (NanoTemper, Germany) (Duhr and Braun, 2006), which allows a highly specific labelling of proteins containing polyhistidine-tags. For protein

labelling, a 100 nM dye solution was prepared by mixing 2 µl of dye (5 µM) with 98 µl Hepes buffer. The protein concentration was adjusted to 200 nM in a total volume of 100 µl. 100 µl of protein (200 nM) were then mixed with 100 µl of dye (100 nM) and incubated in the dark for 30 min at room temperature. The labelled protein was then centrifuged for 10 min at 4 ºC and 15,000 × g.

During sample preparation, a ligand dilution series of galectin-1 was prepared. In total, 16 PCR tubes were used for each interaction measurement. 10 µl of Hepes buffer supplemented with 0.05% Tween-20 were added to tubes 2-16 by reverse pipetting. Samples were prepared as described in 4.4.7 (page 49). For each interaction measurement, a total of 20 µl of 420 µM gal-1 were used.

After incubation, the samples were centrifuged for 10 min at 10,000 × g and loaded into Monolith NT.115 Standard capillaries. The interactions were measured in both conditions: (i) 20% MST power and 40% MST power, and (ii) 40% MST power and 40% LED power. The time settings were 5 sec fluorescence before, 30 sec MST on, 5 sec fluorescence after, with 25 sec delay. Sample preparation and measurements were done in triplicates, unless stated otherwise. Data was collected using NT.Control Software and analysed by MO.Affinity analysis using expert mode.

5. Results

5.1. Recombinant expression of Galectin-1

A major aim of the work was the preparation of a histidine tag-less cysteine-less mutant construct of Galectin-1 (hereinafter designated pOPINE_CSGal-1_STOP) followed by recombinant expression and purification of the resulting mutant protein, CSGal-1. The mutant protein was subjected to stability testing by nano-DSF, assessment of particle size distribution profile by DLS, and analysis of sugar-binding by label-free MST. Importantly, a preliminary comparative analysis between mutant CSGal-1 and wild-type Gal-1, kindly provided by Petr Pachl, Ph.D., was also initiated using the aforementioned biophysical techniques.

5.1.1. Construction of CSGal-1 expression vector

The construct encoding for a tag-less cysteine-less mutant form of galectin-1 was designed by Nishi and colleagues (Nishi et al., 2008). The construct is based on the known nucleotide sequence encoding for wild-type galectin-1, in which the authors introduced changes aiming at the improvement of the properties of the resultant recombinant protein. As seen in Figure 8 (page 53), the amino terminal methionine residue corresponding to the start codon was removed – an alteration naturally occurring in Gal-1 molecule; in addition, all the cysteine residues were replaced by serine residues in a sequence of site-directed mutagenesis steps.

The expression construct was obtained by amplification and insertion of a DNA fragment encoding for CSGal-1 into a linearized pOPINE vector by Infusion cloning reaction. The cloned construct was analysed by agarose gel electrophoresis (Figure 9; page 53). The resolved band coincided with the expected molecular size of pOPINE_CSGal-1_STOP (5556 bp).

wtGal-1

atggcttgtggtctggtcgccagcaacctgaatctcaaacctggagagtgccttcgagtgcgaggcgagg
tggctcctgacgctaagagcttcgtgctgaacctgggcaaagacagcaacaacctgtgcctgcacttcaa
ccctcgcttcaacgcccacggcgacgccaacaccatcgtgtgcaacagcaaggacggcggggcctggggg
accgagcagcgggaggctgtctttcccttccagcctggaagtgttgcagaggtgtgcatcaccttcgacc
aggccaacctgaccgtcaagctgccagatggatacgaattcaagttccccaaccgcctcaacctggaggc
catcaactacatggcagctgacggtgacttcaagatcaaatgtgtggcctttgactga

MACGLVASNLNLKPGECLRVRGEVAPDAKSFVLNLGKDSNNLCLHFNPRFNAHGDANTIVCNSKDGGAW
GTEQREAVFPFQPGSVAEVCITFDQANLTVKLPDGYEFKFPNRLNLEAINYMAADGDFKIKCVAFD

CSGal-1

gcttctggtctggtcgccagcaacctgaatctcaaacctggagagagccttcgagtgcgaggcgaggtgg
ctcctgacgctaagagcttcgtgctgaacctgggcaaagacagcaacaacctgagcctgcacttcaaccc
tcgcttcaacgcccacggcgacgccaacaccatcgtgagcaacagcaaggacggcggggcctgggggacc
gagcagcgggaggctgtctttcccttccagcctggaagtgttgcagaggtgagcatcaccttcgaccagg
ccaacctgaccgtcaagctgccagatggatacgaattcaagttccccaaccgcctcaacctggaggccat
caactacatggcagctgacggtgacttcaagatcaaatctgtggcctttgactga

ASGLVASNLNLKPGESLRVRGEVAPDAKSFVLNLGKDSNNLSLHFNPRFNAHGDANTIVSNSKDGGAWGT
EQREAVFPFQPGSVAEVSITFDQANLTVKLPDGYEFKFPNRLNLEAINYMAADGDFKIKSVAFD

Figure 8 – Nucleotide and amino acid sequences of wild-type and cysteine-less mutant of Galectin-1. Representation of start codon (underlined and highlighted in yellow), highlighted sequence differences (in yellow) and stop codon (in red). Adapted from (Nishi et al., 2008).

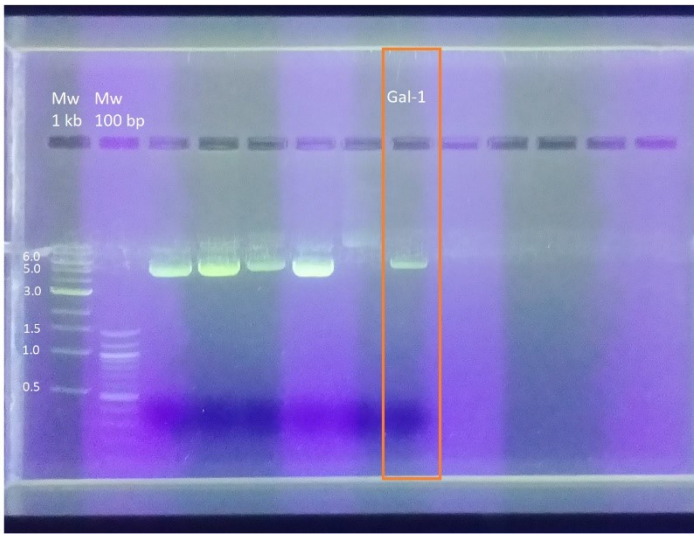

Figure 9 – Agarose gel electrophoresis of pOPINE_CSGal-1_STOP expression plasmid. Electrophoresis of the expression plasmid (marked as Gal-1 in the figure) with the expected size of 5556 bp. Two DNA ladders were used – Mw 1 kb and Mw 100 bp. The remaining lanes refer to unrelated samples.

5.1.2. Recombinant expression and purification of CSGalectin-1 mutant

Recombinant expression of CSGal-1 was initiated by transforming *E. coli* BL21(DE3) cells with the plasmid pOPINE_CSGal-1_STOP. One transformed colony was randomly selected and used to prepare a starter culture. After overnight growth, a small volume of the starter culture was transferred to a larger volume of LB medium supplemented with carbenicillin. The cells were incubated until the measured optical density at 550 nm was in the 0.4 to 0.8 range, followed by induction with 0.5 mM IPTG and incubation at 20ºC overnight. The following day the cells were harvested, and the purification of the protein was initiated by enzymatic lysis. Purification of CSGal-1 was then continued by affinity chromatography using a lactose-sepharose column (Figure 10; page 54). The protein of interest was isocratically eluted with Tris buffer supplemented with lactose and Ca^{2+} ions.

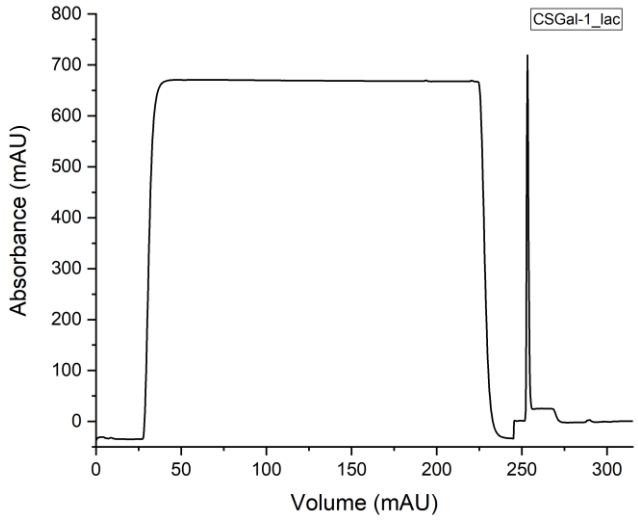

Figure 10 – Chromatogram from affinity chromatography of mutant CSGalectin-1. The initial step in the purification of CSGal-1 was affinity chromatography using a Lactose-Sepharose column. The protein of interest was eluted in a complexed form with lactose.

The fractions collected from the peak of elution were concentrated and further purified by size-exclusion chromatography (Figure 11; page 55). Since CSGal-1 was eluted from affinity chromatography in a complexed form with lactose, the next step in purification consisted of the removal of the sugar from the protein. In order to do so, the SEC column (Superdex 200 Increase 10/300 GL) was equilibrated with Tris buffer supplemented with

EDTA; the property of EDTA as a chelating agent was thus used in order to break the coordination of Ca^{2+} ions required for the maintenance of the protein:sugar complex, consequently releasing CSGal-1 from the lactose molecules.

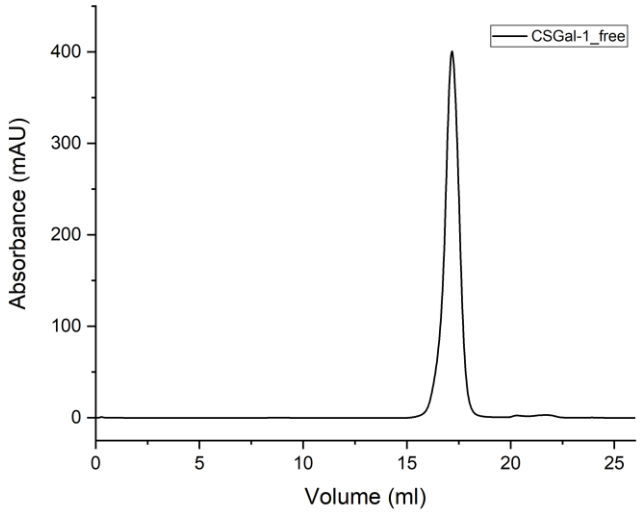

Figure 11 – Chromatogram of size-exclusion chromatography of CSGalectin-1. Lactose removal by SEC using Superdex 200 Increase 10/300 GL, Buffer 4 (Tris with EDTA). CSGal-1 was eluted in an unbound form.

The following step in the purification protocol served two major purposes: first, the recharging of the protein with Ca^{2+} ions, and second, the exchange of buffer into Hepes buffer. The formation of protein:protein and protein:sugar complexes is dependent on the coordination of Ca^{2+} ions, and since the previous purification step depleted the protein of the ions this step is of crucial importance. Buffer exchange into Hepes buffer is an additional important step for the preparation of the samples for the subsequent biophysical assays, since the techniques used require all the experimental components to be in the same buffer. Both purposes were achieved by purification of the protein into Hepes buffer supplemented with Ca^{2+} ions by size-exclusion chromatography using HiTrap desalting columns (Figure 12; page 56).

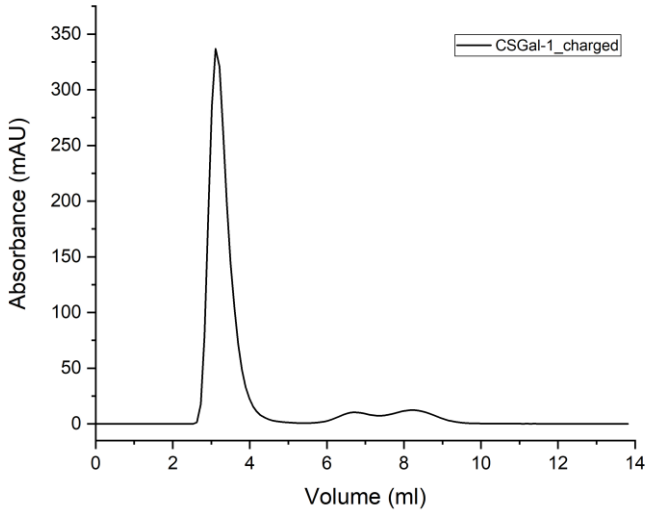

Figure 12 – Chromatogram of size-exclusion chromatography employed for protein recharging and buffer exchange. The protein of interest was eluted in Hepes buffer supplemented with 10 mM $CaCl_2$. The obtained protein fraction was designated CSGal-1_charged.

The fractions corresponding to the peak of elution were analysed by SDS-PAGE (Figure 14; page 58), concentrated to approximately 7 mg/ml, and stored at 4ºC until further use.

5.1.3. Wild-type Galectin-1 preparation

The quality of CSGal-1 mutant protein both in a general term and more specifically in the engagement with NK cell receptors was assessed in a comparative analysis with wild-type galectin-1. A stock solution of recombinant wtGal-1 was kindly provided by Petr Pachl, Ph.D., from IOCB of the CAS, Prague. wtGal-1 was expressed in *Escherichia coli* BL21(DE3) and purified by IMAC and SEC. The protein was stored in PBS buffer containing β-mercaptoethanol at 4ºC until further use.

This protein construct of wild-type Gal-1 has five extra N-terminal amino acid residues remaining from the signal sequence (Ser-Asn-Ala-Ala-Ser), following the sequence shown in Figure 8 (page 53).

Similar to the purification of the mutant protein, wild-type Galectin-1 was additionally prepared for further biophysical assays by buffer exchange into Hepes buffer using size-exclusion chromatography (Figure 13; page 57). The exchange into a non-reducing buffer was of vital importance since wtGal-1 was used in MST interaction studies with NK cell receptors which are sensitive to reducing conditions.

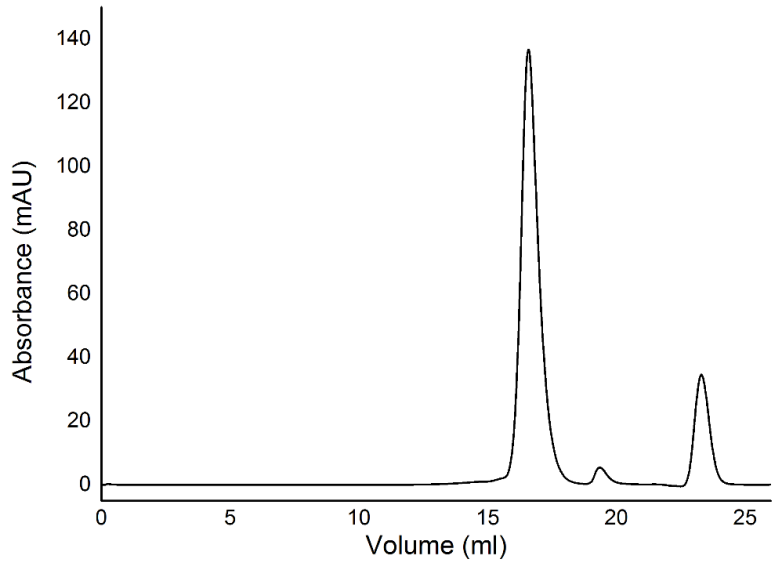

Figure 13 – Chromatogram from size-exclusion chromatography of wtGal-1 using Superdex 200 Increase 10/300 GL. Wild-type Galectin-1 was purified by SEC in order to exchange the storage buffer into Hepes buffer. The main peak at approximately 17.5 ml corresponds to the elution of the protein of interest which has an expected molecular weight of cca 15 kDa.

5.1.4. Galectin-1 protein quality control

Prior to the start of the binding assays by microscale thermophoresis, the quality of both wild-type and cysteine-less mutant galectin-1 was assessed by a combination of techniques, ranging from SDS-PAGE, dynamic light scattering, nano differential scanning fluorimetry, analytical ultracentrifugation and label-free microscale thermophoresis.

5.1.4.1. SDS-PAGE

The collected SEC fractions were analysed by SDS-PAGE (Figure 14; page 58); the fractions corresponding to the peak of elution were concentrated as previously described to the final concentration of approximately 7 mg/ml. The exchange of the storage buffer (PBS buffer with β-mercaptoethanol) into a non-reducing buffer (Hepes buffer) was always done as close as possible to the initiation of the next experiments so as to avoid conservation of wtGal-1 in non-reducing conditions, which is known to hinder the ability of the protein to participate in protein:protein and protein:sugar interactions.

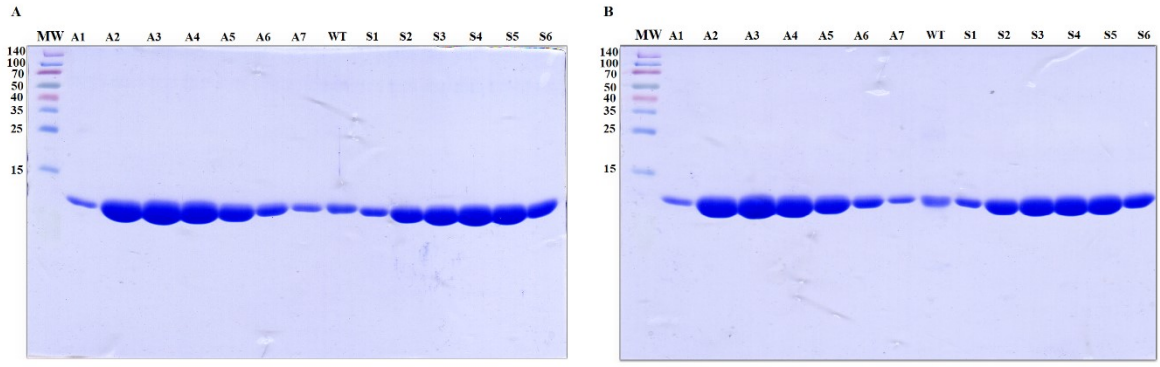

Figure 14 – SDS-PAGE analysis of wild-type and mutant Galectin-1. 15% polyacrylamide gel under reducing (A) and non-reducing conditions (B). Samples A1 to A7 correspond to the peak fractions from affinity chromatography used for purification of mutant CSGal-1. The resulting concentrated fraction of buffer exchange by SEC of wild-type Galectin-1 was used as a control. Fractions S1 to S6 correspond to fractions from step in purification of the mutant protein subsequent to lactose removal. All the fractions show a single band and an apparent molecular weight below 15 kDa, which is expected.

5.1.4.2. Dynamic Light Scattering

The quality of the recombinantly expressed and purified proteins was initially verified by dynamic light scattering, where the particle size distribution and dispersity were analysed. Each protein sample was measured four times using the default mode and one time using multi-angle dynamic light scattering at 25ºC and with an equilibration time of 120 s to default temperature in between measurements. DLS was measured for both wtGal-1 (Figure 15; page 59) and CSGal-1 (Figure 16; page 59). The mutant protein was measured in three different conditions: CSGal-1 bound to lactose in the presence of Ca^{2+} (CSGal-1_lac), CSGal-1 without lactose and Ca^{2+} ions (CSGal-1_free) and Ca^{2+}-charged lactose-free CSGal-1 (CSGal-1_charged), data only shown for CSGal-1_charged.

The data was collected and processed using ZS Xplorer Software (Malvern Panalytical, *UK*). For data processing the default General Purpose analysis model was used.

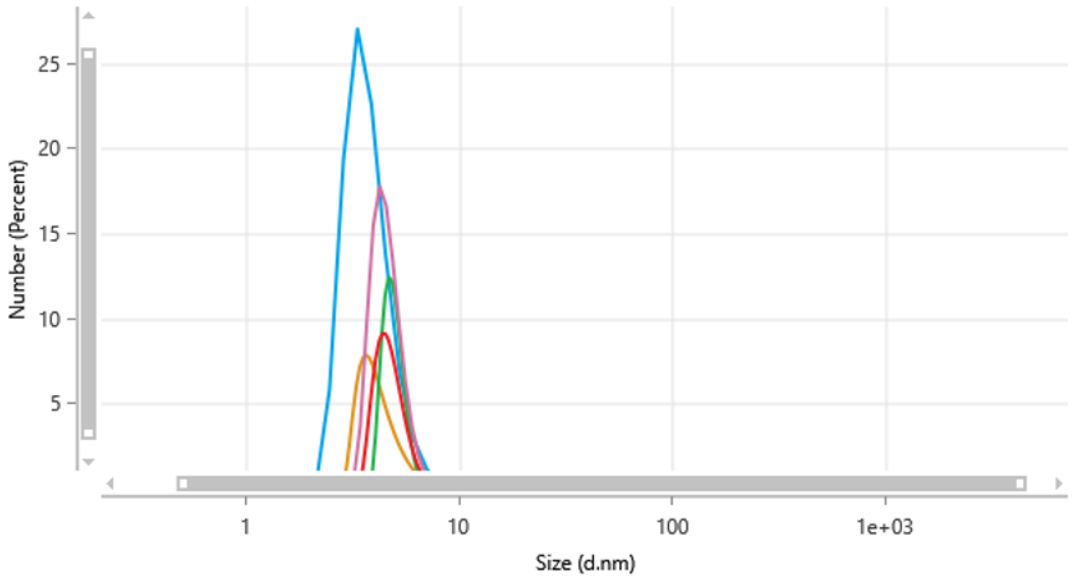

Figure 15 – Dynamic light scattering analysis for wtGal-1. Representation of particle size distribution by number (percent) in function of particle size (d.nm) of wtGal-1. The four default measurements are shown in blue, green, yellow, and red; the measurement using multi-angle dynamic light scattering is shown in pink.

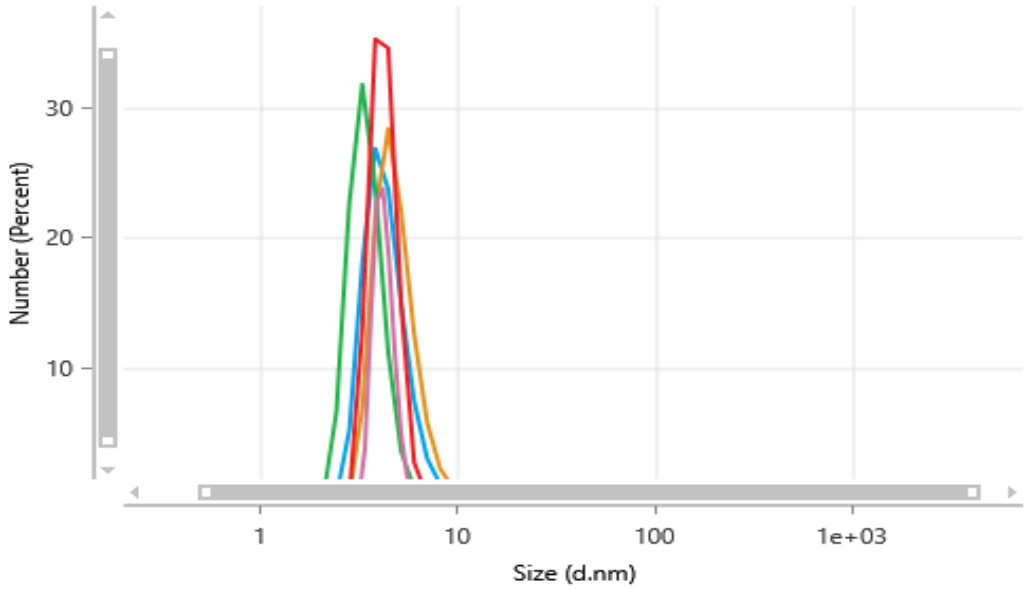

Figure 16 – Dynamic light scattering analysis for CSGal-1_charged. Representation of particle size distribution by number in function of particle size of mutant CSGal-1_charged. The default measurements are shown in blue, green, yellow, and red; multi-angle dynamic light scattering measurement is shown in pink.

Both proteins have the same behaviour in terms of light scattering properties. Both wtGal-1 and CSGal-1_charged seem to be monodisperse particles of the size between 5-10 nm.

5.1.4.3. Nano Differential Scanning Fluorimetry

The thermal stability was assessed by nano differential scanning fluorimetry in native conditions. Changes in the intrinsic fluorescence of CSGal-1_lac, CSGal-1_free, CSGal-1_charged and wtGal-1 were measured using Prometheus NT.48 (NanoTemper, Germany). NanoDSF data was gathered at two wavelengths (330 and 350 nm). The plot of the ratio of the two wavelengths in function of temperature was used to obtain information on the thermal unfolding of the proteins. A more precise calculation of the melting temperature of the samples was obtained by deducing the first derivative from the previous plot. Although not the main aim when employing the technique, the aggregation of the samples was also assessed as a function of temperature (Figure 17; page 61).

The nano DSF shows a reduced thermal stability of all forms of cysteine-less mutant galectin-1 in comparison to the wild-type protein. The differences between the obtained melting temperatures of individual states of the mutant protein are negligible, indicating that presence or absence of lactose or Ca^{2+} ions does not influence protein stability. Analysis of protein scattering in function of increasing temperature have shown that wild-type galectin-1 starts forming aggregates right after unfolding at approximately 70 ºC.

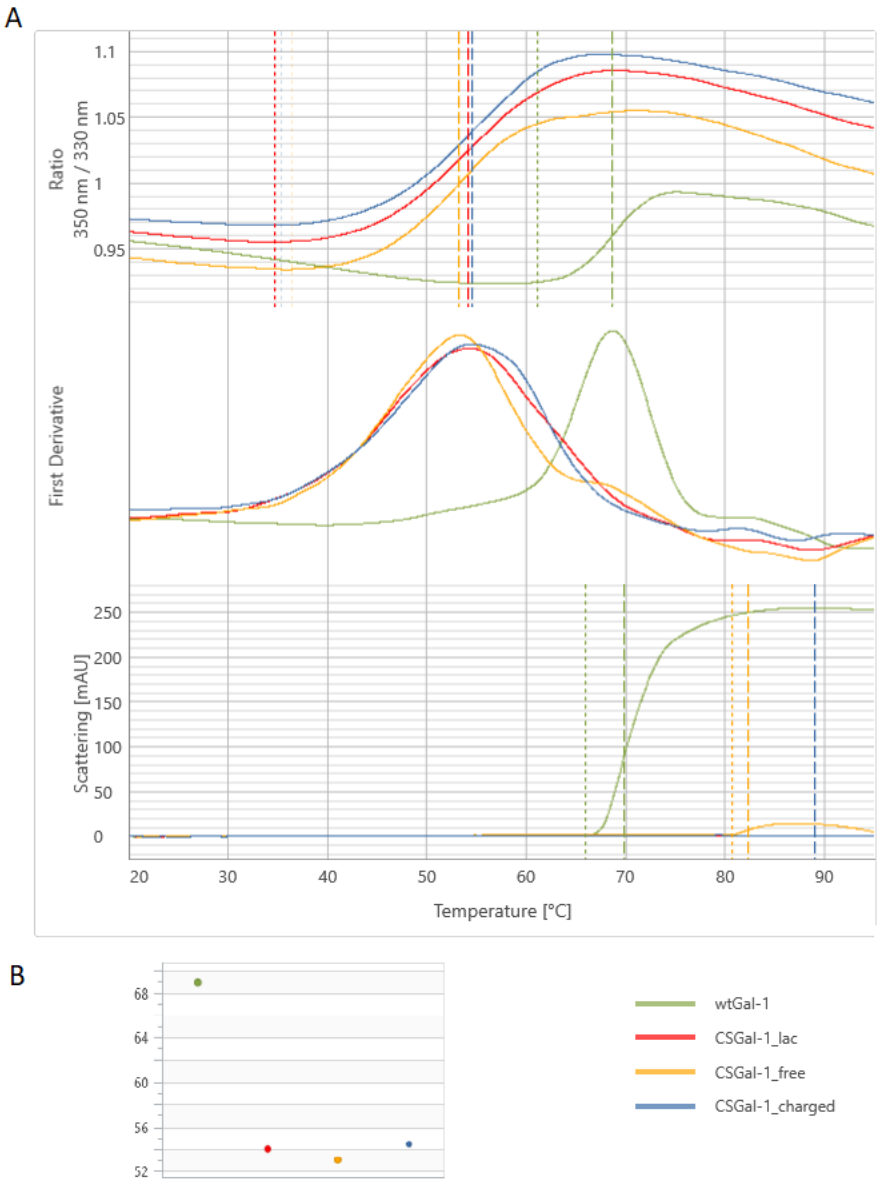

Figure 17 – Quantitative analysis of thermal unfolding of wild-type and mutant forms of Galectin-1 by nano differential scanning fluorimetry. (A) Shown first are the progress curves where the ratio of 330 and 350 nm wavelengths is plotted against temperature. The second graph shows the first derivative calculated from the previous progress curves; the second derivative plot provides a more precise method for the determination of the melting temperatures. The last shown plot is displaying the scattering in function of temperature, where protein aggregation is analysed. **(B)** Detailed view of obtained melting temperatures for each measured protein. The data was collected by PT.ThermControl and analysed by PR.StabilityAnalysis.

5.1.4.4. Analytical Ultracentrifugation

The quality of the recombinantly expressed cysteine-less mutant galectin-1 was additionally verified by a sedimentation velocity experiment using analytical ultracentrifugation. In this experiment, the protein homogeneity, dispersity, and possible aggregation, were evaluated.

The obtained sedimentation profile of the mutant protein was thus compared with the profile for wild-type galectin-1 so as to provide another means of quality assessment.

The data was collected and processed by SENDTERP and SEDFIT software programs.

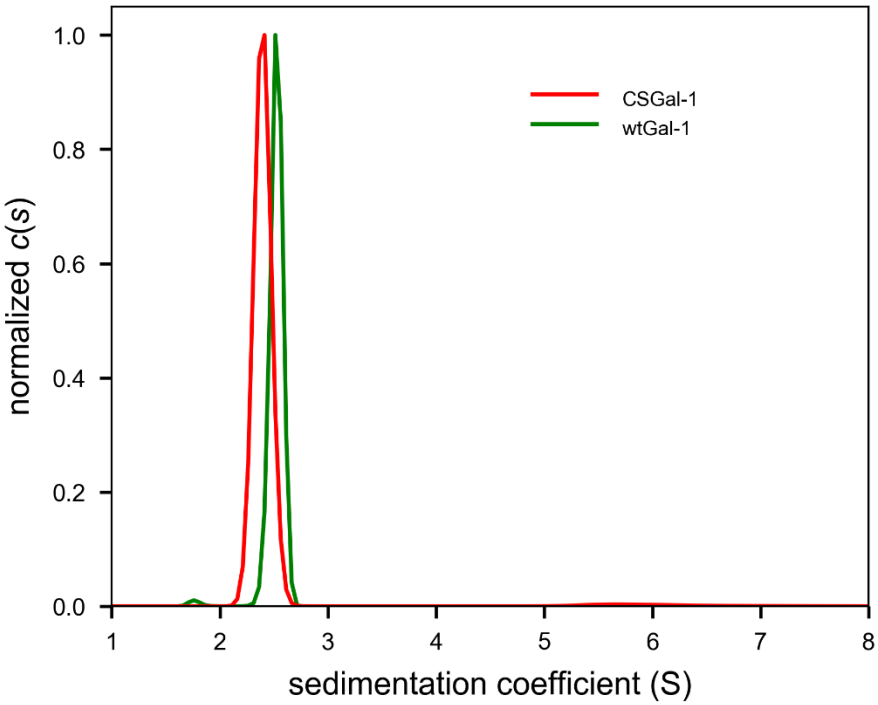

Figure 18 – Comparative sedimentation analysis of wild-type and cysteine-less mutant Galectin-1. Representation of plots of normalized distributions c(s) in function of sedimentation coefficient (S; Svedberg unit) for wtGal-1 (green) and CSGal-1 (red).

The data shows a monodisperse population between 2-3 S corresponding to the dimeric form of both proteins. The CSGal-1 distribution was shown to be shifted to slightly lower sedimentation coefficients. An additional difference between the sedimentation profiles of mutant and wild-type galectin-1 is the presence of a smaller population below 2 S for wtGal-1, possibly corresponding to the monomeric form of the protein.

5.1.4.5. Label-free Microscale Thermophoresis

The last step in the analysis of the quality of the recombinantly expressed proteins was label-free MST in which the sugar-binding abilities of the protein were tested. The interaction of CSGal1_charged (i.e., mutant galectin-1 charged with Ca^{2+} ions) with lactose was measured in native conditions.

Before label-free MST, a pre-test was done in which the buffers, ligands, and target proteins were measured at 20% MST 80% LED powers in order to determine the intrinsic fluorescence of each component used in the experimental setup.

Following optimisation of the experimental conditions, the final setup was determined as follows: CSGal-1_charged with the final concentration of 500 nM with lactose as an interaction partner with a concentration starting at 2.5 mM; lactose was titrated in a 1:1 ratio in a series of 16 samples. Lactose solution was prepared in Hepes buffer supplemented with 10 mM $CaCl_2$, so as to avoid the decrease of the concentration of Ca^{2+} ions required for the interaction to occur.

Each measurement was measured in triplicate at 20% MST power and 80% LED power with the time settings 5 s fluorescence before, 30 s MST on, and 5 s fluorescence after. The data was collected using NT.Control Software and analysed using Expert Mode by MO.Affinity Analysis Software. For data analysis the selected cold region was from -01.00 s to 0.00 s; the hot region selected was from 0.50 s to 1.5 s. The analysed binding profile is shown in Figure 19.

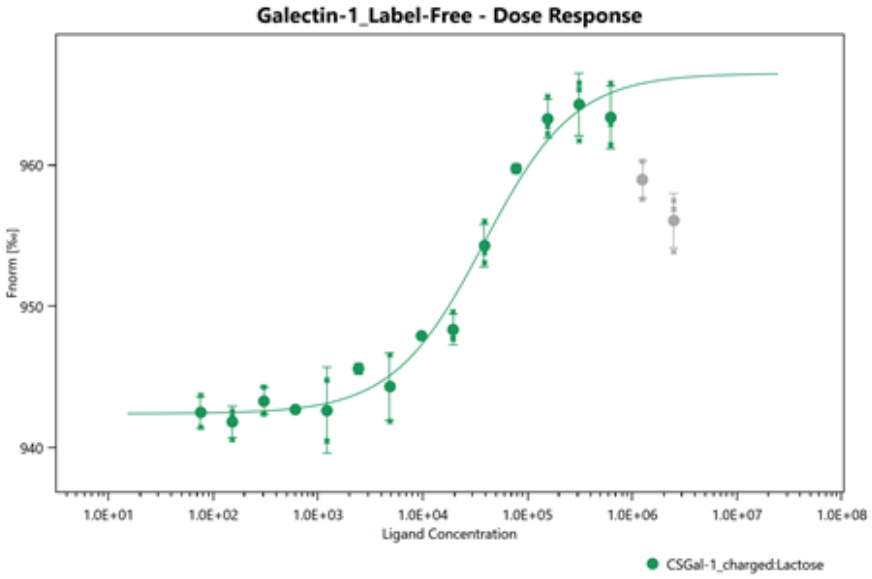

Figure 19 – Analysed result from label-free MST experiment of CSGal-1_charged interaction with lactose. Binding curve of a titration of lactose at concentrations from 625 µM to 76 nM against 500 nM CSGal-1 is shown. The fitted data yielded a K_d of 40 ± 7 µM, with standard error of regression 1.369. The data was fitted using the K_d fit in the 1.5 s time preset using expert mode in MO.Affinity Analysis software. The error bars represented the standard deviation calculated from three independent label-free measurements.

The points corresponding to the highest lactose concentration (i.e., 1.25 mM and 2.5 mM) were excluded from K_d analysis. The fitted data yielded a dissociation constant of approximately 40 ± 7 µm with a standard error of regression of 1.369. These values are comparable to previously published data for wild-type galectin-1 (K_d ~ 50 µM) (Ahmad et al., 2004; Nesmelova et al., 2010).

5.2. Recombinant expression and characterization of NK cell receptors

An important aim of the project was the validation of the putative interaction of the NK cell receptor CD69 with Galectin-1 as proposed by de la Fuente and colleagues (de la Fuente et al., 2014). In order to study the putative binding of CD69 with Gal-1, two different constructs encoding for the ectodomain of CD69 were expressed in HEK293 cells and purified by IMAC and SEC. The two constructs were prepared and described elsewhere by RNDr. Ondřej Vaněk, Ph.D. (Vaněk et al., 2008). CD69_CM1 is a longer construct of CD69 containing five more amino acid residues than CD69_C2; CD69_CM1 has an additional cysteine residue known to be involved in homodimer formation. Both constructs have two predicted N-glycosylation sites and a polyhistidine tag at the C-terminus (Figure 20).

```
CD69_CM1        ETGQYNCPGQYTFSMPSDSHVSSCSEDWVGYQRKCYFISTVKRSWTSAQNACSEHGATLA
CD69_C2         ETG-----GQYTFSMPSDSHVSSCSEDWVGYQRKCYFISTVKRSWTSAQNACSEHGATLA

CD69_CM1        VIDSEKDMNFLKRYAGREEHWVGLKKEPGHPWKWSNGKEFNNWFNVTGSDKCVFLKNTEV
CD69_C2         VIDSEKDMNFLKRYAGREEHWVGLKKEPGHPWKWSNGKEFNNWFNVTGSDKCVFLKNTEV

CD69_CM1        SSMECEKNLYWICNKPYKGTKHHHHHH
CD69_C2         SSMECEKNLYWICNKPYKGTKHHHHHH
```

Figure 20 – Pairwise sequence alignment of CD69_C2 and CD69_CM1 constructs using EMBOSS Needle. Represented are the E terminal amino acid residue from signal sequence (in green), TG residues from cloning site (in grey), GTK residues from cloning site (in red). N-glycosylation sites (in purple), polyhistidine tag (in blue), and cysteine residues (in yellow) are additionally shown. The last amino acids from CD69 sequence are PYK (in teal).

5.2.1. Recombinant expression and purification of CD69

Two CD69 constructs – pHLsec_CD69_CM1 and pHLsec_CD69_C2 – were initially transiently transfected in HEK293T cell line for the expression of both forms of the receptor with wild-type glycosylation. The productions were harvested a week after the transient transfection and the total production volume (200 ml) was purified by immobilized metal affinity chromatography using HiTrap Talon 5 ml column. The fractions corresponding to

the peak of elution were collected and concentrated to the final volume of approximately 750 µl using Amicon Ultra concentrators. The concentrated fraction was purified by size-exclusion chromatography using Superdex 200 10/300 GL columns (Figure 21). The chromatographies were performed on HPLC system ÄKTA Basic. The SEC fractions were resolved and analysed by SDS-PAGE.

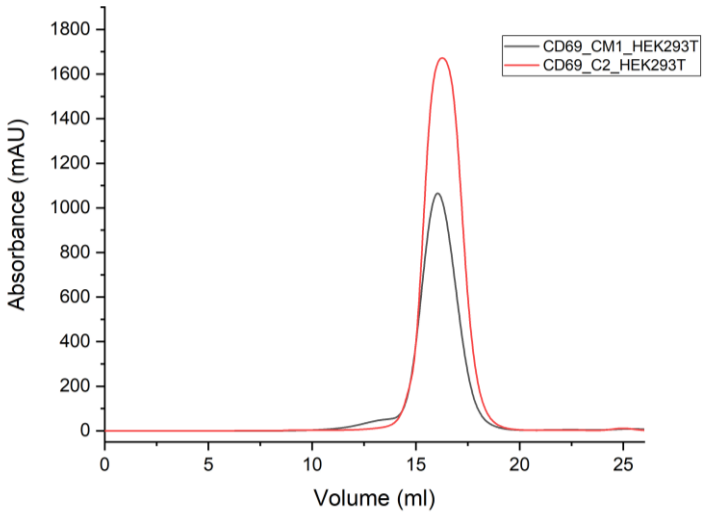

Figure 21 – Chromatogram of size-exclusion chromatography using Superdex 200 Increase 10/300 GL of CD69_C2 and CD69_CM1 expressed in HEK293T cell line. Several fractions were collected in both chromatographies with the total yield for CD69_CM1 and CD69_C2 being 8.8 mg/ml and 4.2 mg/ml, respectively.

Using the same expression and purification approach as previously described, CD69_CM1 and CD69_C2 were expressed in HEK293S GnTI$^-$ cell line in order to have expressed proteins with homogeneous glycosylation. The proteins were then purified by IMAC and SEC (data only shown for CD69_C2) (Figure 22; page 66) and resolved by SDS-PAGE.

For the study of the dependency on the N-glycan moiety in the interaction between CD69 and Gal-1, both CD69 constructs expressed in HEK293S GnTI$^-$ cells were enzymatically deglycosylated with endoglycosidase F. The deglycosylated proteins were further purified by SEC in order to separate the glycoforms from the remaining components in solution (i.e., enzyme and protein fractions that were not fully glycosylated) (data only shown for CD69_C2) (Figure 22; page 66). The SEC fractions were resolved by SDS-PAGE in reducing and non-reducing conditions (data not shown).

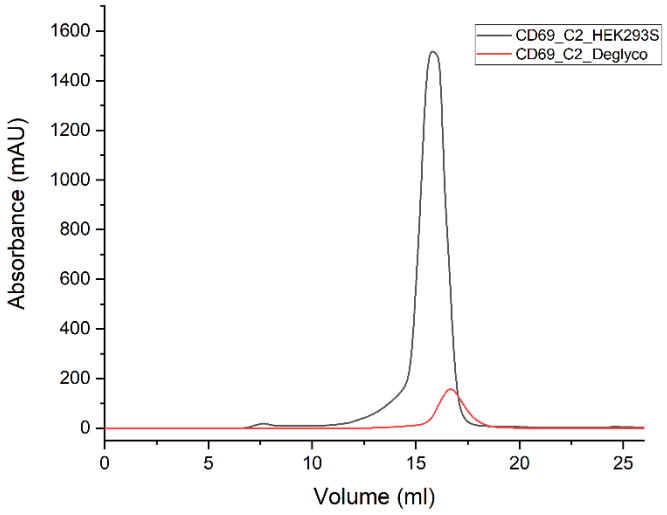

Figure 22 – Chromatogram of size-exclusion chromatography of CD69_C2 expressed in HEK293S cells and deglycosylated form of CD69 using Superdex 200 Increase 10/300 GL column. Chromatogram of CD69_C2 glycoform with homogeneous glycosylation expressed in HEK293S GnTI$^-$ and of CD69_deglyco which was resultant from the enzymatic deglycosylation of a fraction from the purification of CD69_C2.

5.2.2. CD69 protein quality control

Before the start of binding assays by microscale thermophoresis, the quality of the expressed NK cell receptors was assessed by dynamic light scattering. The dispersity and particle distribution of the samples was analysed also for other NK cell receptors prior to the continuation of the experiments (data only shown for CD69_C2_HEK293T) (Figure 23). DLS data shows a monodisperse population of CD69 with particle size between 5-10 nm.

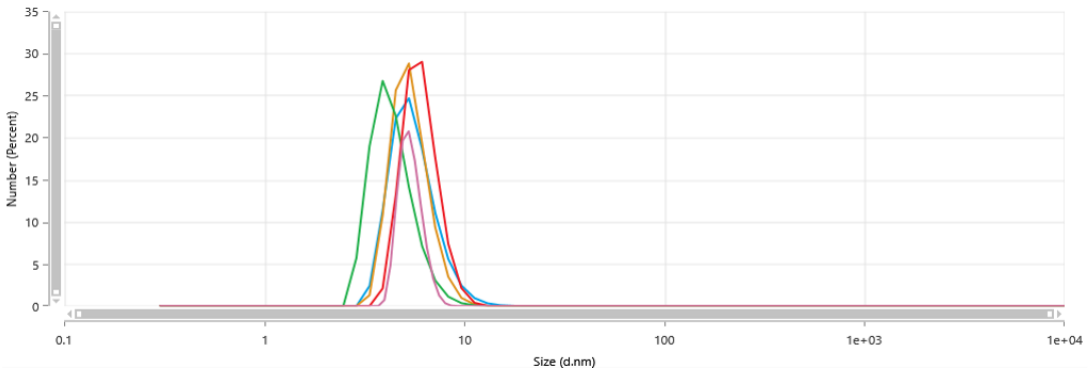

Figure 23 – Representation of results from dynamic light scattering analysis for CD69_C2 expressed in HEK293T cells. Represented are the four default measurements (in blue, green, yellow, and red) and the single multi-angle dynamic light scattering measurement (in pink).

5.3. Study of protein:protein interactions

The putative interaction between NK cell receptor CD69 and wtGalectin-1 was studied by standard microscale thermophoresis. The obtained results using CD69 expressed with wild-type glycosylation in interaction with wtGal-1 pointed towards a confirmation of the proposed binding partner for the receptor. Following the initial MST results, the interaction was further studied on the basis of the presence of a varying N-glycan moiety on the surface of the NK cell receptor. The obtained results pointed once again towards the confirmation of a glycosylation-dependent interaction between CD69 and wtGal-1. To further develop the characterization of the interaction, the same experimental setup was used in the study of wild-type Galectin-1 binding to NK cell receptors related to CD69 either by family or structure.

5.3.1. Study of N-glycan moiety dependency in CD69:wtGal-1 interaction

The study of N-glycan moiety dependency in CD69:Gal-1 interaction was assessed by microscale thermophoresis. Three different glycoforms of CD69_C2 were prepared: (i) CD69 with wild-type glycosylation (CD69_C2_HEK293T); (ii) CD69 with homogeneous glycosylation (CD69_C2_HEK293S); and (iii) enzymatically deglycosylated CD69 (CD69_C2_deglyco) (Figure 24; page 68). In a similar manner, three glycoforms of CD69_CM1 were additionally prepared so that the influence of the construct length in the protein:ligand interaction could also be analysed to some extent (Figure 25; page 68).

The NK cell receptor glycoforms were labelled using a His-tag-specific labelling kit and incubated for 30 min. A titration series of wtGal-1 was prepared in a 1:1 manner with Hepes buffer supplemented with 0.05% Tween-20. In total 16 samples were prepared for each measurement. The labelled proteins were added to the titrated wtGal-1 and incubated for 30 min at room temperature in the dark prior to the measurements. Following incubation, the samples were measured in 40% MST power and 40% LED power using the time settings 5 s fluorescence before, 30 s MST on, and 5 s fluorescence after. The data was collected using NT.Control software and analysed using MO.AffinityAnalysis software in expert mode. For statistical significance each sample was prepared and measured in triplicate unless stated otherwise. The parameters obtained from the fitted data are show in Table 1 (page 69).

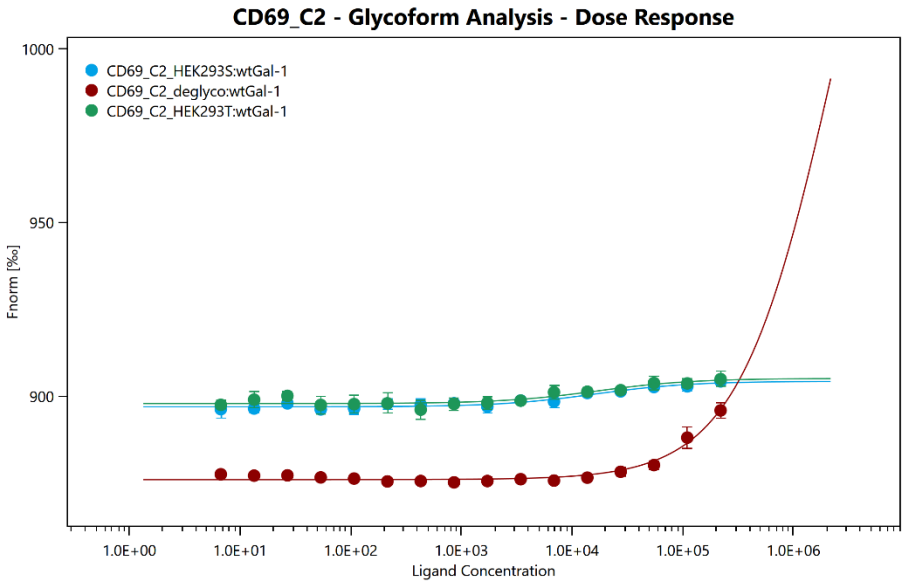

Figure 24 – Thermophoretic analysis of the interaction between CD69_C2 glycoforms with wtGal-1. Changes in thermophoresis of a titration of wtGal-1 at concentrations from 210 µM to 6 nM against 50 nM His-tag labelled CD69_C2 glycoforms are shown. CD69 glycoform library includes protein with wild-type glycosylation (HEK293T), homogeneous $GlcNAc_2Man_5$ glycosylation (HEK293S), and enzymatically deglycosylated (deglyco). The fit yielded a K_d of 16.7 ± 8 µM, 16 ± 5 µM, and 2.45 ± 5.2 mM, respectively. The error bars represented the standard deviation of each data point calculated from three independent thermophoresis measurements.

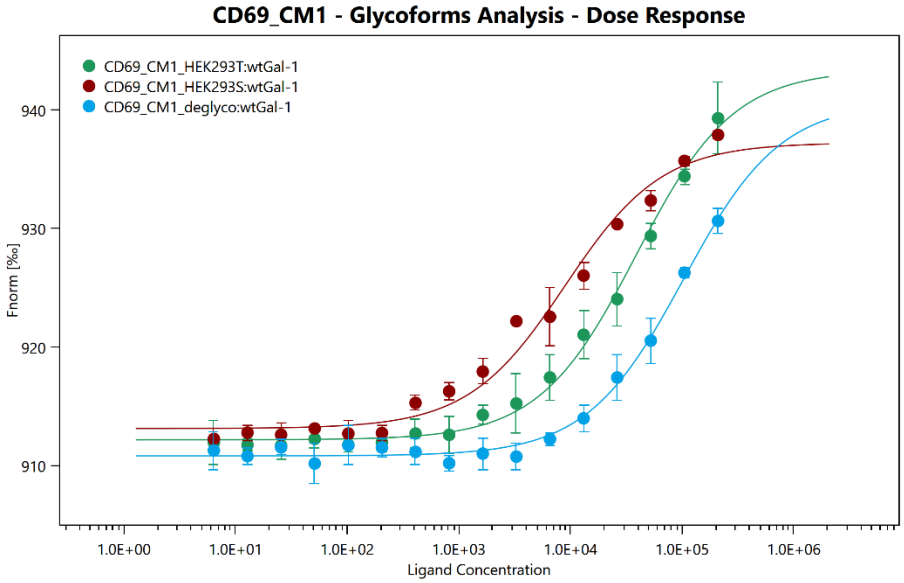

Figure 25 – Thermophoretic analysis of the interaction between CD69_CM1 glycoforms with wtGal-1. Changes in the thermophoretic profile of a titration of wtGal-1 at concentrations from 210 µM to 6 nM against 50 nM His-tag labelled CD69_CM1 glycoforms are shown. The change in thermophoretic signal leads to a K_d fit of 38.8 ± 3.7 µM, 8.9 ± 1.5 µM, and 103 ± 16 µM, respectively starting from wild-type, to homogeneous, and lastly deglycosylated glycoforms. The error bars represent a standard deviation of each data point calculated from three independent measurements.

Table 1 – Parameters obtained from the study of N-glycan dependency on CD69 interaction with wild-type Galectin-1

Sample	K_d (μM)	K_d Confidence (μM)	Standard Error of Regression
CD69_C2_HEK293T	16.7	8.4	1.001
CD69_C2_HEK293S	16.1	5.3	0.6689
CD69_C2_deglyco	2451.8	5267.7	0.9978
CD69_CM1_HEK293T	38.8	3.7	0.6576
CD69_CM1_HEK293S	8.9	1.5	1.270
CD69_CM1_deglyco	103.3	16.0	0.6165

The measured dissociation constants point towards a dependency of the interaction on the presence of N-glycan moieties. Both deglycosylated forms of CD69 have significantly lower affinities than glycosylated proteins. Proteins with homogenous glycosylation were shown to have higher affinities for both CD69 constructs than the wild-type counterparts.

5.3.2. Study of other NK cell receptor interaction with wtGal-1

Following the assessment of protein quality and the confirmation of a glycosylation-dependent interaction between wild-type Galectin-1 and NK cell receptor CD69, the focus shifted towards the study of other putative interactions between different NK cell receptors and wild-type Galectin-1. The same experimental setup as previously described for microscale thermophoresis was used in this study. Members of the CLEC 2 family of NK cell receptors were analysed (i.e., LLT1, KACL, and rCLRB). In addition, NKp30 (a receptor belonging to the NCR family) was also analysed so as to assess the interaction of Galectin-1 with other NK cell receptor families to a small extent. All proteins were expressed in HEK293T cell line thus having a wild-type N-glycan moiety on their surfaces.

In a similar manner to what was previously reported for CD69, the remaining NK cell receptors were purified by IMAC and SEC (Figure 26; page 70). The obtained protein fractions were resolved and analysed by SDS-PAGE.

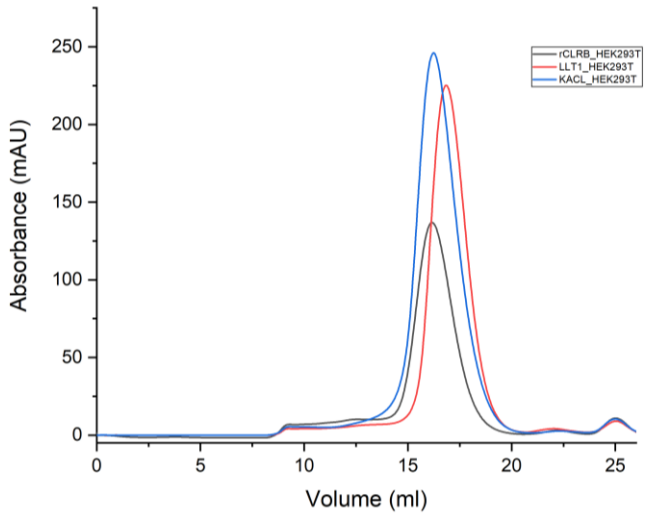

Figure 26 – Chromatogram of size-exclusion chromatography for other NK cell receptors. Elution profiles for the members of the CLEC 2 receptor family, rCLRB, LLT1, and KACL; Superdex 200 Increase 10/300 GL column.

Binding assays of the interaction of wild-type galectin-1 with the remaining NK cell receptors was similarly analysed by microscale thermophoresis (Figure 27). The obtained binding parameters from the fitted data are shown in Table 2 (page 71).

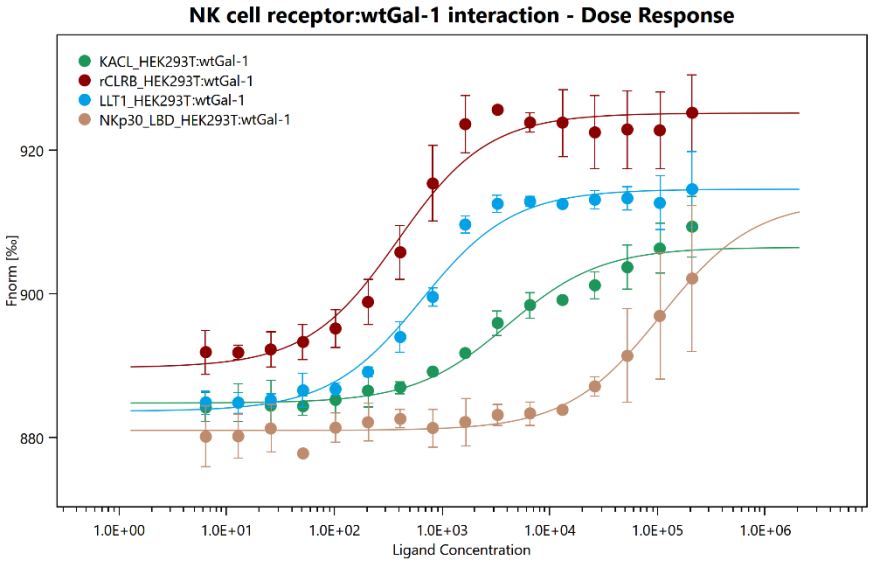

Figure 27 – Analysis of thermophoretic profile of the interaction between different NK cell receptors with wtGal-1. The changes in thermophoresis from the interaction of wtGal-1 with concentration from 210 µM to 6 nM against 50 nM His-tag labelled NK cell receptors are shown. All receptors were expressed in HEK293T cell line. The calculated fit yielded a K_d of 4 ± 0.8 µM, 360 ± 79 nM, 614 ± 106 nM, and 107 ± 30 µM, respectively. The error bars represent the standard deviation from each data point. The error bars from KACL was calculated from three independent measurements (n = 3), with the remaining NK cell receptors being measured in two independent measurements (n = 2).

Table 2 – Parameters obtained from the MST analysis of the NK cell receptor interaction with wild-type Galectin-1

Sample	K_d (nM)	K_d Confidence (nM)	Standard Error of Regression
KACL_HEK293T	4015	848	1.475
rCLRB_HEK293t	362	79	2.455
LLT1_HEK293T	614	106	1.737
NKp30_LBD_HEK293T	107 564	30 555	1.177

Data obtained from the study of the interaction of wild-type galectin-1 with the remaining analysed members from the CLEC 2 family, has shown an increased affinity for the lectin in comparison to what was previously observed for CD69. The interaction of wtGal-1 with NCR receptor NKp30 was shown to have a considerably lower affinity comparable in order to the values obtained for deglycosylated forms of CD69.

5.3.3. Preliminary analysis of CSGal-1 interaction with NK cell receptors

Subsequent of the assessment of the overall quality of the recombinantly expressed cysteine-less mutant galectin-1, a preliminary analysis of its interaction with NK cell receptors was initiated by microscale thermophoresis experiments (Figure 28).

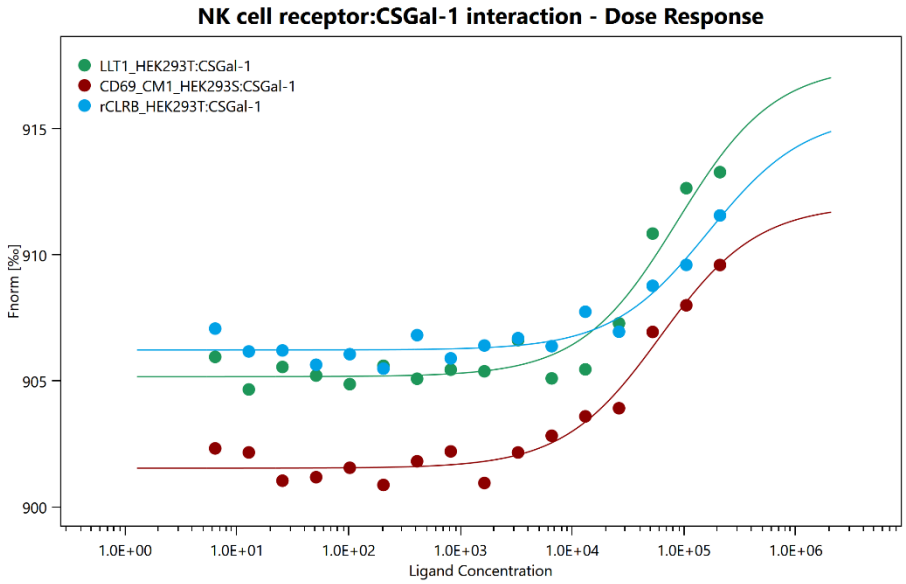

Figure 28 – Preliminary analysis of thermophoretic profile of NK cell receptor interaction with cysteine-less mutant Galectin-1. Changes in MST profile of a titration of CSGal-1 at concentrations from 210 µM to 6 nM against 50 nM His-tag labelled NK cell receptors are shown. The NK cell receptors analysed were LLT1 and rCLRB with wild-type glycosylation, and CD69_CM1 with homogeneous glycosylation. Data shown only for one preliminary measurement.

6. Discussion

The initial assumption of the project was based on the proposed putative glycosylation-dependent interaction of NK cell receptor CD69 with galectin-1 as described by de la Fuente and colleagues in 2014. In order to study the proposed interaction at a biophysical and biochemical level, several approaches were taken into consideration.

The major initial aim was the establishment of an expression and purification protocol for galectin-1. In this part of the project two different forms of the protein were prepared – a wild-type and a cysteine-less mutant protein. Both the establishment of the expression construct and the expression and purification protocol were successfully implemented. CSGal-1 was expressed in *Escherichia coli* BL21(DE3) strain at 20 ºC overnight following IPTG induction. The mutant protein was purified by Lactose-Sepharose affinity chromatography on the basis of its lectin activity. The known affinity of CSGal-1 for lactose was exploited with the aim of capturing the protein by the immobilized carbohydrate matrix. Competitive elution with excess lactose was used for the elution of the protein fractions. The yield from affinity chromatography was approximately 20 mg of protein per 1 litre of bacterial production.

Next, the protein was subjected to the removal of the bound lactose molecules by size-exclusion chromatography. The previously established protein:sugar interaction was disrupted by the incubation and elution of the protein with Tris buffer supplemented with EDTA. The size-exclusion chromatogram depicted in Figure 11 (page 55) shows a single peak at approximately 17.5 ml which corresponds to the elution of the protein in a monomeric form (the expected molecular weight is approximately 14.6 kDa). A direct consequence of the removal of lactose by chelating the Ca^{2+} ions with EDTA was the depletion of the protein of the ions, which are known to be vital in the establishment of protein interactions with both proteins and sugars. Therefore, the last step in protein purification was the recharging and the exchange of buffer of the mutant protein, both accomplished by a single size-exclusion chromatography. The chromatogram, depicted in Figure 12 (page 56), shows a major peak corresponding to the elution of the protein of interest; in addition, two smaller broad peaks can be seen at approximately 6 to 9 ml, which could be a result of the presence of impurities.

Regarding wild-type galectin-1 the purification protocol consisted only of buffer exchange by size-exclusion chromatography (Figure 13; page 57). As seen in the chromatogram, a

major main peak at approximately 17.5 ml corresponds to the elution of wtGal-1. Aside from the main peak, two smaller peaks are also observed which could result from remnant particles from protein expression or from the storage conditions in which the protein was kept. Nevertheless, both CSGal-1 and wtGal-1 appear to be eluted in a similar way with both proteins having an elution volume of approximately 17.5 ml. The resulting fractions of CSGal-1 from affinity chromatography and size-exclusion chromatography, and the concentrated wtGal-1 fraction from buffer exchange were resolved and analysed by SDS-PAGE (Figure 14; page 58). Analysis of the polyacrylamide gels in both reducing and non-reducing conditions show a single band for all the resolved protein fractions and a similar migration pattern for both mutant and wild-type proteins. The initial comparative analysis of CSGal-1 with wtGal-1 by chromatographic techniques points towards a strong similarity between both proteins.

The expressed proteins were further characterized by a range of biophysical techniques in which different properties were assessed. The initial assessment was done by dynamic light scattering in which the protein dispersity and the particle size distribution were analysed. As shown in Figure 15 and Figure 16 (page 59), all the measurements for both wild-type and cysteine-less mutant show a monodisperse population. In addition, the particle diameter is below 10 d.nm which is expected for particles with molecular weight similar to that of galectin-1.

The next step in protein characterization was the assessment of thermal stability and protein aggregation by nano differential scanning fluorimetry in which the intrinsic fluorescence of the proteins was used for measurements in native conditions. The thermal unfolding of wild-type galectin-1 and the mutant (in three different stages of purification) was measured by detecting shifts of fluorescence intensity at 330 and 350 nm in a temperature gradient.

As shown in Figure 17 (page 61), CSGal-1_lac, CSGal-1_free, and CSGal-1_charged have melting temperatures of approximately 54 ºC, with some minor variations in between measurements. The form of the mutant without lactose and without Ca^{2+} ions (CSGal-1_free), although by a small degree, has the lowest melting temperature of the three measured samples which indicates a possible stabilization of the protein by Ca^{2+}-mediated interaction with lactose. Interestingly, the wild-type protein has a melting temperature of approximately 68 ºC; a 12 ºC difference in comparison with the measured thermal unfolding for the mutant forms. As described by López-Lucendo and colleagues (López-Lucendo et

al., 2004), the fold of galectin-1 involves a β-sandwich consisting of two antiparallel β-sheets of five (F1-F5) and six (S1-S6a/b) strands, respectively, that are involved in the maintenance of the homodimer integrity. Four hydrogen bonds formed between Val5 and Ser7 residues from both S1 strands in the anterior face, and five hydrogen bonds involving residues Lys129, Phe133, and Val131 from the F1 strands in the opposing face stabilize the protein dimer. In addition, the involvement of Leu4, Ala6, and Leu9 from S1, and Ile128, Val131, and Phe133 from F1 strands further stabilize the homodimer by the formation of a hydrophobic core.

Comparative analysis of the three-dimensional crystal structures of wtGal-1 (PDB code IGZW) and CSGal-1 (PBD code 2ZKN) shows small changes in Leu9 and Phe133 residues in the cysteine-less mutant. Residues Lys129 and Asp123 show very similar conformations, only with slight changes in comparison with wild-type conformation. The observed displacements in the amino acid residues involved in protein stabilization present a possible explanation for the differences observed in the thermal unfolding of wtGal-1 and CSGal-1 observed by nano differential scanning fluorimetry.

An additional possible explanation lies on the amino acid replacement of cysteine residues by serine residues in the cysteine-less mutant form of galectin-1. Wild-type galectin-1 has six cysteine residues (Cys2, Cys16, Cys42, Cys60, Cys88, and Cys130 in PBD structure 1GWZ) that are possibly involved in spontaneous intramolecular disulphide bonding. In CSGal-1 the serine residues replacing Cys residues adopt a similar side-chain conformation in the majority of cases, with the exception of Ser16 and Ser43 (in PBD structure 2ZKN) that engage in hydrogen bonding. Structural data by Lopéz-Lucendo and colleagues shows that Cys16 and Cys88 are readily available for intramolecular disulphide bonding, whereas Cys130 could be involved in homodimer formation by intermolecular disulphide bonding (López-Lucendo et al., 2004). The fact that Cys16 has been replaced by Ser16 in CSGal-1 and that the serine residue is engaged in interactions other than intramolecular disulphide bonding could explain to some extent the apparent decrease stability of the mutant protein in comparison with the wild-type galectin-1.

Another possible explanation could lie on the purification protocol established for CSGal-1. The protein is initially purified by Lactose-Sepharose affinity chromatography followed by a step of lactose removal by SEC, in which the Ca^{2+}-dependent lactose interaction is disrupted through EDTA addition, with the last step consisting of protein recharging. The

removal of lactose and depletion of Ca^{2+} ions from the expressed protein could affect the stability of the mutant protein. Nevertheless, analysis of the progress curves of thermal unfolding of the mutant protein in three different purification stages (i.e., CSGal-1_lac, CSGal-1_free, and CSGal-1_charged) shows a similar behaviour in all the measurements. This implies that the mutant protein, regardless of the purification step, has an impaired stability when compared with wild-type galectin-1.

Besides the data provided on the thermal unfolding of galectin-1, nano DSF also provided some information on the possible protein aggregation by analysis of scattering pattern of the proteins. Interestingly, wild-type galectin-1 started aggregating at lower temperatures than any of the CS mutant forms. A possible explanation lies on oxidation-induced protein aggregation. As shown by Nishi and colleagues (Nishi et al., 2008), CSGal-1 is resistant to oxidation in the absence of a reducing agent, whereas wild-type Gal-1 is prone to oxidation if stored in non-reducing conditions. Therefore, the exchange of the storage buffer from PBS buffer supplemented with β-mercaptoethanol to Hepes buffer prior to the biophysical analyses could explain the apparent higher sensitivity to aggregation than expected.

The recombinantly expressed mutant protein was further analysed and compared with wtGal-1 by analytical ultracentrifugation. The resulting graph represented in Figure 18 (page 62) shows a major population corresponding to the formation of a stable homodimer in both protein distributions. In addition, the distribution for wtGal-1 also shows a minor population corresponding to the monomeric form of the protein. Interestingly, a shift to the left (corresponding to lower sedimentation coefficients) is also seen for CSGal-1 thus indicating that the protein does not behave in a completely identical manner in solution as wtGal-1 does. A possible explanation lies on the fact that the mutant protein has a different expression construct and purification protocol, which could result in CSGal-1 having slightly different hydrodynamic properties than wtGal-1.

CSGal-1 mutant protein was further analysed regarding its ability to engage in protein:sugar interactions by label-free MST. The data from label-free MST shows a binding curve that decays for the two highest concentrations for lactose. A possible explanation for such behaviour is related to the viscosity of the samples. Protein thermophoresis in a temperature gradient is highly sensitive to the increase of the viscosity of solutions and therefore the diffusion of molecules is impaired. For the analysis of the data, the two points corresponding to the highest ligand concentration were hidden and the remaining dataset was fitted using

K_d fit model. The obtained binding affinity for lactose ($K_d \sim 40$ μM) is similar to the values for wild-type galectin-1 available in literature (Ahmad et al., 2004; Nesmelova et al., 2010), thus indicating that the replacement of Cys by Ser residues does not appear to impair the carbohydrate-binding activity of the protein.

Following the establishment of an expression and purification protocol and an assessment of quality of cysteine-less mutant galectin-1, the second initial aim was the expression and purification of NK cell receptors (e.g., CD69, KACL, LLT1, and rCLRB) in HEK293 cell lines. In this segment of the project both forms of the NK cell receptor CD69 were expressed in different HEK293 variant cell lines leading to the formation of a glycoform library with glycosylation ranging from wild-type to homogeneous. The fully deglycosylated proteins were obtained after enzymatic deglycosylation with endoglycosidase F, thus complementing the library. The remaining proteins were expressed only in HEK293T cell line.

As seen in the depicted chromatograms (pages 65, 66, and 70) all the proteins were eluted in single peaks corresponding to the elution volumes calculated for the given molecular weights (ranging from approximately 15 to 17 kDa). The quality of the eluted proteins was next analysed by dynamic light scattering (Figure 23; page 66). For all the measurements, a single monodisperse population was seen at the expected particle size and no aggregates were detected, pointing towards the good quality of the expressed proteins.

An important part of the project consisted of the study of galectin-1 interaction with NK cell receptors. The approach to the study was subdivided into: (i) analysis of N-glycan moiety dependency on CD69 interaction with wtGal-1; (ii) analysis of wtGal-1 binding with other NK cell receptors; and (iii) preliminary analysis of CSGal-1 binding to NK cell receptors.

The N-glycan moiety dependency was studied using three glycoforms of CD69 (protein with wild-type, homogeneous, or absent glycosylation) for both constructs by microscale thermophoresis. The results obtained for CD69_C2 point towards a confirmation of a glycosylation-dependent interaction with wtGal-1, as previously described by de la Fuente and colleagues (de la Fuente et al., 2014). The obtained binding affinities for wild-type and homogeneous glycosylated NK cell receptor are rather similar, only with a slightly higher affinity for the later (Table 3; page 77).

Table 3 - Calculated parameters for CD69_C2 interaction with wtGal-1 by MST

Sample	K_d (μM)
CD69_C2_HEK293T	16.7 ± 8.4
CD69_C2_HEK293S	16.1 ± 5.3
CD69_C2_deglyco	2451.8 ± 5267.7

In a similar manner, the interaction of CD69_CM1 with wild-type galectin-1 was also analysed. Confirming the results obtained for the other CD69 protein construct, the analysed interactions show once again the dependency on the presence of a glycan moiety (Table 4; page 78). As described for the previous CD69 construct, the homogeneously glycosylated NK cell receptor showed once again a higher binding affinity for the lectin than the wild-type glycosylated CD69. Interestingly, the K_d values from the fitted data for CD69_CM1_HEK293T and CD69_CM1_HEK293S are approximately double and half, respectively, of the values obtained for both glycoforms of CD69_C2. The obtained data appears to point towards the formation of a stronger complex of CD69_CM1 with wild-type galectin-1 but only in the presence of homogeneous glycosylation. Despite the increased stability of CD69 in the case of the covalently stabilized construct, the type of glycosylation on its surface appears to be the deciding factor whether the formed complex has higher or lower binding affinity.

The obtained results in this work regarding CD69 interaction with galectin-1 show nevertheless a decreased binding affinity than the values available in literature. The NK cell receptor was shown to have an interaction in the micromolar range at best, in contrary to the nanomolar range interaction described by de la Fuente and colleagues (de la Fuente et al., 2014). The discrepancy between the data could be a result of the constructs used in the measurements. Both CD69 constructs were optimised in the basis of its purification, therefore the introduced changes might impair to some extent the interaction with galectin-1. A possible additional explanation lies on the fact that the parameters were obtained using two different techniques. de la Fuente and colleagues studied the interaction of CD69 with wtGal-1 using surface plasmon resonance in which recombinant CD69 was fused with an Fc fragment and immobilized on the sensor chip for the measurements. Both fusion and immobilization are stabilizing factors in complex formation, thus possibly explaining the higher obtained affinities.

Table 4 – Obtained parameters for MST measurement of the interaction of wtGal-1 with CD69_CM1 glycoforms

Sample	K_d (μM)
CD69_CM1_HEK293T	38.8 ± 3.7
CD69_CM1_HEK293S	8.9 ± 1.5
CD69_CM1_deglyco	103.3 ± 16.0

Following the confirmation of a glycosylation-dependent interaction between wild-type galectin-1 and NK cell receptor CD69, other NK cell receptors were equally analysed as putative binding partners of wtGal-1. The receptors selected for the study included other members of the CLEC 2 family (e.g., LLT1, KACL, and rCLRB) and a receptor belonging to the NCR family of NK cell receptors (NKp30). An initial assessment of sequence (Figure 29) and structure similarity (Figure 30; page 79) of the CLEC 2 members was done by software specialized in similarity-based analyses. LLT1, KACL, and rCLRB amino acid sequences were aligned to CD69_CM1 sequence. The structures of the receptors were manipulated and analysed using Pymol software. In a similar manner to sequence alignment, the structures were aligned to CD69 structure using Pymol.

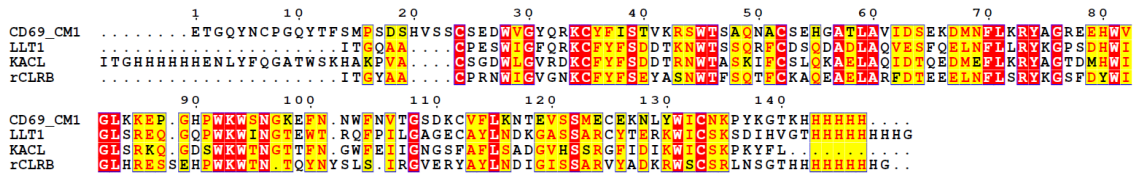

Figure 29 – Sequence alignment of CD69_CM1, LLT1, KACL, and rCLRB prepared by T-Coffee Expresso and ESPript. Every tenth residue of the CD69_CM1 sequence are indicated. Conserved residues are highlighted in yellow (>70 % conservation) or red (>100 % conservation).

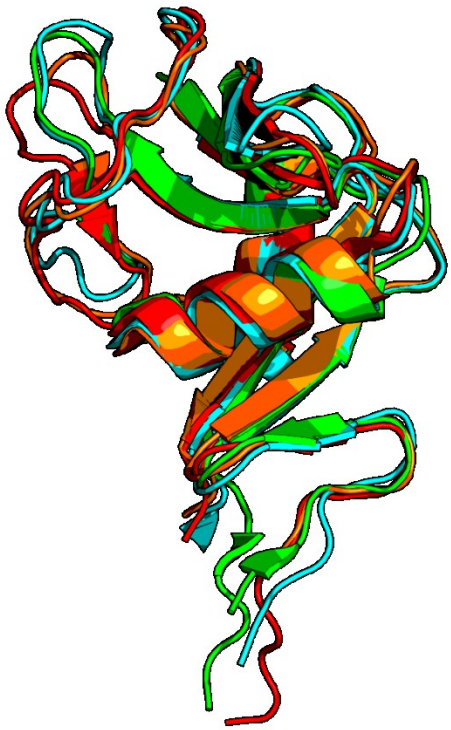

Figure 30 – Structural alignment of monomeric CD69_CM1, LLT1, KACL, and rCLRB molecules. View of CD69_CM1 (red; PBD: 3HUP), LLT1 (green; PBD: 4QKG), KACL (orange; PDB: 4IOP), and rCLRB (blue; PDB: 6E7D), illustrating the similarity of the three-dimensional structures. The PBD structures were manipulated and aligned by structure using Pymol 1.8.2.0.

Figure 29 depicts the sequence alignment of the NK cell receptors where several amino acids are shown to be highly conserved (in red) or with conservative replacements (in yellow). With the exception of some amino acids in the N- and C-termini, the remaining amino acid residues are conserved to some extent thus highlighting the similarity between the amino acid sequences of the receptors. The structural alignment shown in Figure 30, shows a maintenance in the overall spatial organisation of the receptors. The two α-helices and the β-strands appear to be highly conserved in all structures, with only evident structural changes in the loops. NKp30 sequence and structure were not compared with the remaining features of the mentioned NK cell receptors since the receptor belongs to a different NK cell receptor family and therefore a lower degree of similarity was expected.

So as to further understand the interaction of wild-type galectin-1 with NK cell receptors a series of binding assays by microscale thermophoresis were performed. In the series of experiments, the influence of N-glycosylation site number was preliminarily analysed by the

study of NKp30 interaction with the lectin. In addition, the interaction was also analysed on the basis of protein-dependency in complex formation.

As shown in Table 5, the fitted data from the interaction of wtGal-1 with NKp30 showed a considerably weak affinity, similar in range to the values obtained for the deglycosylated forms of CD69, thus indicating that the higher number of N-linked glycosylation chains does not appear to increase the affinity between the proteins (NKp30 has three N-glycosylation sites). Interestingly, KACL, rCLRB, and LLT1 were shown to bind wild type-Galectin-1 with a higher affinity than described for CD69. Therefore, in these conditions, the lectin appears to behave as a putative binding ligand for these receptors as well. The interaction of galectin-1 with these receptors indicates a possible stabilization of the complex by specific amino acid residues. For complementing the presented data, the analysis of the N-glycan moiety dependency and the description of the putative amino acid residues in the stabilization of the formed complex should also be done.

Table 5 – Parameters from the MST analysis of the NK cell receptor interaction with wtGal-1

Sample	K_d (nM)
KACL_HEK293T	4015 ± 848
rCLRB_HEK293t	362 ± 79
LLT1_HEK293T	614 ± 106
NKp30_LBD_HEK293T	107 564 ± 30 555

With the gathered information regarding the studied interaction systems, the ability of CSGal-1 in the engagement into protein:protein interactions was also preliminarily assessed by microscale thermophoresis. A series of three single measurements of the mutant protein in interaction with CD69_CM1_HEK293S, LLT1_HEK293T and rCLRB_HEK293T receptors (shown in Figure 28; page 71) shows a shift in the ligand binding curve to the right pointing towards a lower binding affinity.

For further research, the ability of CSGal-1 mutant to engage in protein:protein interactions should be assessed by a range of complementary techniques. In relation to the CD69:wtGal-1 interaction, further characterization with an array of biophysical techniques ought to be done in order to understand in a more detailed manner the properties required for protein interaction and complex formation. In a similar way, the interaction with other NK cell receptors should be further characterized since galectin-1 might correspond as well

to a putative binding ligand. The ultimate goals in the project are the mechanistic and structural description of the interaction of NK cell receptors with galectin-1 and the study of the interactions in a biological context.

7. Conclusion

- Cysteine-less mutant of galectin-1 was successfully expressed in *E. coli* BL21(DE3) and purified by Lactose-Sepharose affinity chromatography and SEC.

- NK cell receptors were expressed in HEK293 cell lines and a glycoform library of CD69 was created.

- Recombinantly expressed proteins were characterized by DLS, nano DSF, AUC, and label-free MST.

- Interaction between CD69 and wild-type galectin-1 was confirmed and shown to be glycosylation-dependent.

- Novel interactions of wild-type galectin-1 with other NK cell receptors were described.

8. References

Ahmad, N., Gabius, H.-J., Sabesan, S., Oscarson, S., and Brewer, C.F. (2004). Thermodynamic binding studies of bivalent oligosaccharides to galectin-1, galectin-3, and the carbohydrate recognition domain of galectin-3. Glycobiology *14*, 817–825.

Angata, T., and Brinkman-Van der Linden, E.C.M. (2002). I-type lectins. Biochim. Biophys. Acta BBA - Gen. Subj. *1572*, 294–316.

Bankovich, A.J., Shiow, L.R., and Cyster, J.G. (2010). CD69 suppresses sphingosine 1-phosophate receptor-1 (S1P1) function through interaction with membrane helix 4. J. Biol. Chem. *285*, 22328–22337.

Bartel, Y., Bauer, B., and Steinle, A. (2013). Modulation of NK Cell Function by Genetically Coupled C-Type Lectin-Like Receptor/Ligand Pairs Encoded in the Human Natural Killer Gene Complex. Front. Immunol. *4*.

Bashirova, A.A., Martin, M.P., McVicar, D.W., and Carrington, M. (2006). The Killer Immunoglobulin-Like Receptor Gene Cluster: Tuning the Genome for Defense. Annu. Rev. Genomics Hum. Genet. *7*, 277–300.

Blom, B., and Spits, H. (2006). Development of Human Lymphoid Cells. Annu. Rev. Immunol. *24*, 287–320.

Bonilla, F.A., and Oettgen, H.C. (2010). Adaptive immunity. J. Allergy Clin. Immunol. *125*, S33–S40.

Boyton, R.J., and Altmann, D.M. (2007). Natural killer cells, killer immunoglobulin-like receptors and human leucocyte antigen class I in disease. Clin. Exp. Immunol. *149*, 1–8.

Brown, G.D., Willment, J.A., and Whitehead, L. (2018). C-type lectins in immunity and homeostasis. Nat. Rev. Immunol. *18*, 374–389.

Camby, I., Le Mercier, M., Lefranc, F., and Kiss, R. (2006). Galectin-1: a small protein with major functions. Glycobiology *16*, 137R-157R.

Campbell, K.S., and Purdy, A.K. (2011). Structure/function of human killer cell immunoglobulin-like receptors: lessons from polymorphisms, evolution, crystal structures and mutations. Immunology *132*, 315–325.

Cedeno-Laurent, F., Barthel, S.R., Opperman, M.J., Lee, D.M., Clark, R.A., and Dimitroff, C.J. (2010). Development of a Nascent Galectin-1 Chimeric Molecule for Studying the Role of Leukocyte Galectin-1 Ligands and Immune Disease Modulation. Doi.Org 4659–4672.

Chiffoleau, E. (2018). C-Type Lectin-Like Receptors As Emerging Orchestrators of Sterile Inflammation Represent Potential Therapeutic Targets. Front. Immunol. *9*.

Cibrián, D., and Sánchez-Madrid, F. (2017). CD69: from activation marker to metabolic gatekeeper. Eur. J. Immunol. *47*, 946–953.

Clark, R., and Kupper, T. (2005). Old Meets New: The Interaction Between Innate and Adaptive Immunity. J. Invest. Dermatol. *125*, 629–637.

Colucci, F., Caligiuri, M.A., and Di Santo, J.P. (2003). What does it take to make a natural killer? Nat. Rev. Immunol. *3*, 413–425.

Cooper, D.N., and Barondes, S.H. (1990). Evidence for export of a muscle lectin from cytosol to extracellular matrix and for a novel secretory mechanism. J. Cell Biol. *110*, 1681–1691.

Cyster, J.G., and Schwab, S.R. (2012). Sphingosine-1-Phosphate and Lymphocyte Egress from Lymphoid Organs. Annu. Rev. Immunol. *30*, 69–94.

Dahms, N.M., and Hancock, M.K. (2002). P-type lectins. Biochim. Biophys. Acta BBA - Gen. Subj. *1572*, 317–340.

Dambuza, I.M., and Brown, G.D. (2015). C-type lectins in immunity: recent developments. Curr. Opin. Immunol. *32*, 21–27.

Di Lella, S., Sundblad, V., Cerliani, J.P., Guardia, C.M., Estrin, D.A., Vasta, G.R., and Rabinovich, G.A. (2011). When Galectins Recognize Glycans: From Biochemistry to Physiology and Back Again. Biochemistry *50*, 7842–7857.

Diefenbach, A., and Raulet, D.H. (2001). Strategies for target cell recognition by natural killer cells. Immunol. Rev. *181*, 170–184.

Diehl, G.E., Yue, H.H., Hsieh, K., Kuang, A.A., Ho, M., Morici, L.A., Lenz, L.L., Cado, D., Riley, L.W., and Winoto, A. (2004). TRAIL-R as a Negative Regulator of Innate Immune Cell Responses. Immunity *21*, 877–889.

Dodd, R.B., and Drickamer, K. (2001). Lectin-like proteins in model organisms: implications for evolution of carbohydrate-binding activity. Glycobiology *11*, 71R-9R.

Drickamer, K. (1999). C-type lectin-like domains. Curr. Opin. Struct. Biol. *9*, 585–590.

Drickamer, K., and Fadden, A.J. (2002). Genomic analysis of C-type lectins. Biochem. Soc. Symp. 59–72.

Duhr, S., and Braun, D. (2006). Why molecules move along a temperature gradient. Proc. Natl. Acad. Sci. U. S. A. *103*, 19678–19682.

Fauriat, C., Long, E.O., Ljunggren, H.-G., and Bryceson, Y.T. (2010). Regulation of human NK-cell cytokine and chemokine production by target cell recognition. Blood *115*, 2167–2176.

Fehniger, T.A., Cooper, M.A., Nuovo, G.J., Cella, M., Facchetti, F., Colonna, M., and Caligiuri, M.A. (2003). CD56bright natural killer cells are present in human lymph nodes and are activated by T cell–derived IL-2: a potential new link between adaptive and innate immunity. Blood *101*, 3052–3057.

Feng, C., Woodside, K.J., Vance, B.A., El-Khoury, D., Canelles, M., Lee, J., Gress, R., Fowlkes, B.J., Shores, E.W., and Love, P.E. (2002). A potential role for CD69 in thymocyte emigration. Int. Immunol. *14*, 535–544.

Ferlazzo, G., Tsang, M.L., Moretta, L., Melioli, G., Steinman, R.M., and Münz, C. (2002). Human Dendritic Cells Activate Resting Natural Killer (NK) Cells and Are Recognized via the NKp30 Receptor by Activated NK Cells. J. Exp. Med. *195*, 343–351.

Flexner, S., and Noguchi, H. (1902). Snake venom in relation to haemolysis, bacteriolysis, and toxicity. J. Exp. Med. *6*, 277–301.

Freud, A.G., Becknell, B., Roychowdhury, S., Mao, H.C., Ferketich, A.K., Nuovo, G.J., Hughes, T.L., Marburger, T.B., Sung, J., Baiocchi, R.A., et al. (2005). A Human CD34(+) Subset Resides in Lymph Nodes and Differentiates into CD56brightNatural Killer Cells. Immunity *22*, 295–304.

de la Fuente, H., Cruz-Adalia, A., Martinez Del Hoyo, G., Cibrián-Vera, D., Bonay, P., Pérez-Hernández, D., Vázquez, J., Navarro, P., Gutierrez-Gallego, R., Ramirez-Huesca, M., et al. (2014). The leukocyte activation receptor CD69 controls T cell differentiation through its interaction with galectin-1. Mol. Cell. Biol. *34*, 2479–2487.

Gasteiger, E., Hoogland, C., Gattiker, A., Duvaud, S., Wilkins, M.R., Appel, R.D., and Bairoch, A. (2005). Protein Identification and Analysis Tools on the ExPASy Server. In The Proteomics Protocols Handbook, J.M. Walker, ed. (Totowa, NJ: Humana Press), pp. 571–607.

Hanna, J., Goldman-Wohl, D., Hamani, Y., Avraham, I., Greenfield, C., Natanson-Yaron, S., Prus, D., Cohen-Daniel, L., Arnon, T.I., Manaster, I., et al. (2006). Decidual NK cells regulate key developmental processes at the human fetal-maternal interface. Nat. Med. *12*, 1065–1074.

Hauri, H.-P., Appenzeller, C., Kuhn, F., and Nufer, O. (2000). Lectins and traffic in the secretory pathway. FEBS Lett. *476*, 32–37.

Hayashizaki, K., Kimura, M.Y., Tokoyoda, K., Hosokawa, H., Shinoda, K., Hirahara, K., Ichikawa, T., Onodera, A., Hanazawa, A., Iwamura, C., et al. (2016). Myosin light chains 9 and 12 are functional ligands for CD69 that regulate airway inflammation. Sci. Immunol. *1*, eaaf9154–eaaf9154.

Herberman, R.B., Nunn, M.E., Holden, H.T., and Lavrin, D.H. (1975). Natural cytotoxic reactivity of mouse lymphoid cells against syngeneic and allogeneic tumors. II. Characterization of effector cells. Int. J. Cancer *16*, 230–239.

Hudspeth, K., Silva-Santos, B., and Mavilio, D. (2013). Natural Cytotoxicity Receptors: Broader Expression Patterns and Functions in Innate and Adaptive Immune Cells. Front. Immunol. *4*.

Imai, K., Matsuyama, S., Miyake, S., Suga, K., and Nakachi, K. (2000). Natural cytotoxic activity of peripheral-blood lymphocytes and cancer incidence: an 11-year follow-up study of a general population. Lancet Lond. Engl. *356*, 1795–1799.

Johnstone, R.W., Frew, A.J., and Smyth, M.J. (2008). The TRAIL apoptotic pathway in cancer onset, progression and therapy. Nat. Rev. Cancer *8*, 782–798.

Kilpatrick, D.C. (2002). Animal lectins: a historical introduction and overview. Biochim. Biophys. Acta BBA - Gen. Subj. *1572*, 187–197.

Koch, J., Steinle, A., Watzl, C., and Mandelboim, O. (2013). Activating natural cytotoxicity receptors of natural killer cells in cancer and infection. Trends Immunol. *34*, 182–191.

Kolenko, P., Skálová, T., Vaněk, O., Štěpánková, A., Dušková, J., Hašek, J., Bezouška, K., and Dohnálek, J. (2009). The high-resolution structure of the extracellular domain of human CD69 using a novel polymer. Acta Crystallograph. Sect. F Struct. Biol. Cryst. Commun. *65*, 1258–1260.

Kondo, M., Scherer, D.C., King, A.G., Manz, M.G., and Weissman, I.L. (2001). Lymphocyte development from hematopoietic stem cells. Curr. Opin. Genet. Dev. *11*, 520–526.

Kruse, P.H., Matta, J., Ugolini, S., and Vivier, E. (2014). Natural cytotoxicity receptors and their ligands. Immunol. Cell Biol. *92*, 221–229.

Lanier, L.L. (2005). NK cell recognition. Annu. Rev. Immunol. *23*, 225–274.

Laue, T.M., Shah, B.D., Ridgeway, T.M., and Pelletier, S.L. (1992). Computer-aided interpretation of analytical sedimentation data for proteins. Comput.-Aided Interpret. Anal. Sediment. Data Proteins 90–125.

Lee, S.-H., Miyagi, T., and Biron, C.A. (2007). Keeping NK cells in highly regulated antiviral warfare. Trends Immunol. *28*, 252–259.

Leukert, N., Sorg, C., and Roth, J. (2005). Molecular basis of the complex formation between the two calcium-binding proteins S100A8 (MRP8) and S100A9 (MRP14). Biol. Chem. *386*, 429–434.

Lieberman, J. (2010). Granzyme A activates another way to die. Immunol. Rev. *235*, 93–104.

Lin, C.-R., Wei, T.-Y.W., Tsai, H.-Y., Wu, Y.-T., Wu, P.-Y., and Chen, S.-T. (2015). Glycosylation-dependent interaction between CD69 and S100A8/S100A9 complex is required for regulatory T-cell differentiation. FASEB J. Off. Publ. Fed. Am. Soc. Exp. Biol. *29*, 5006–5017.

Liu, F.-T., and Rabinovich, G.A. (2005). Galectins as modulators of tumour progression. Nat. Rev. Cancer *5*, 29.

Ljunggren, H.G., and Kärre, K. (1990). In search of the "missing self": MHC molecules and NK cell recognition. Immunol. Today *11*, 237–244.

López-Cabrera, M., Santis, A.G., Fernández-Ruiz, E., Blacher, R., Esch, F., Sánchez-Mateos, P., and Sánchez-Madrid, F. (1993). Molecular cloning, expression, and chromosomal localization of the human earliest lymphocyte activation antigen AIM/CD69,

a new member of the C-type animal lectin superfamily of signal-transmitting receptors. J. Exp. Med. *178*, 537–547.

López-Cabrera, M., Muñoz, E., Blázquez, M.V., Ursa, M.A., Santis, A.G., and Sánchez-Madrid, F. (1995). Transcriptional regulation of the gene encoding the human C-type lectin leukocyte receptor AIM/CD69 and functional characterization of its tumor necrosis factor-alpha-responsive elements. J. Biol. Chem. *270*, 21545–21551.

López-Lucendo, M.F., Solís, D., André, S., Hirabayashi, J., Kasai, K.I., Kaltner, H., Gabius, H.J., and Romero, A. (2004). Growth-regulatory human galectin-1: Crystallographic characterisation of the structural changes induced by single-site mutations and their impact on the thermodynamics of ligand binding. J. Mol. Biol. *343*, 957–970.

Lucas, M., Schachterle, W., Oberle, K., Aichele, P., and Diefenbach, A. (2007). Dendritic Cells Prime Natural Killer Cells by trans-Presenting Interleukin 15. Immunity *26*, 503–517.

Macauley, M.S., Crocker, P.R., and Paulson, J.C. (2014). Siglec regulation of immune cell function in disease. Nat. Rev. Immunol. *14*, 653–666.

MacFarlane, A.W., and Campbell, K.S. (2006). Signal transduction in natural killer cells. Curr. Top. Microbiol. Immunol. *298*, 23–57.

Moretta, L. (2010). Dissecting CD56dim human NK cells. Blood *116*, 3689–3691.

Moretta, L., Bottino, C., Pende, D., Castriconi, R., Mingari, M.C., and Moretta, A. (2006). Surface NK receptors and their ligands on tumor cells. Semin. Immunol. *18*, 151–158.

Morvan, M.G., and Lanier, L.L. (2016). NK cells and cancer: you can teach innate cells new tricks. Nat. Rev. Cancer *16*, 7–19.

Nakayama, T., Kasprowicz, D.J., Yamashita, M., Schubert, L.A., Gillard, G., Kimura, M., Didierlaurent, A., Koseki, H., and Ziegler, S.F. (2002). The Generation of Mature, Single-Positive Thymocytes In Vivo Is Dysregulated by CD69 Blockade or Overexpression. J. Immunol. *168*, 87–94.

Natarajan, K., Sawicki, M.W., Margulies, D.H., and Mariuzza, R.A. (2000). Crystal structure of human CD69: a C-type lectin-like activation marker of hematopoietic cells. Biochemistry *39*, 14779–14786.

Nesmelova, I.V., Ermakova, E., Daragan, V.A., Pang, M., Menéndez, M., Lagartera, L., Solís, D., Baum, L.G., and Mayo, K.H. (2010). Lactose Binding to Galectin-1 Modulates Structural Dynamics, Increases Conformational Entropy, and Occurs with Apparent Negative Cooperativity. J. Mol. Biol. *397*, 1209–1230.

Nishi, N., Abe, A., Iwaki, J., Yoshida, H., Itoh, A., Shoji, H., Kamitori, S., Hirabayashi, J., and Nakamura, T. (2008). Functional and structural bases of a cysteine-less mutant as a long-lasting substitute for galectin-1. Glycobiology *18*, 1065–1073.

Parkin, J., and Cohen, B. (2001). An overview of the immune system. *357*, 1777–1789.

Pegram, H.J., Andrews, D.M., Smyth, M.J., Darcy, P.K., and Kershaw, M.H. (2011). Activating and inhibitory receptors of natural killer cells. Immunol. Cell Biol. *89*, 216–224.

Pende, D., Parolini, S., Pessino, A., Sivori, S., Augugliaro, R., Morelli, L., Marcenaro, E., Accame, L., Malaspina, A., Biassoni, R., et al. (1999). Identification and molecular characterization of NKp30, a novel triggering receptor involved in natural cytotoxicity mediated by human natural killer cells. J. Exp. Med. *190*, 1505–1516.

Peterson, M.E., and Long, E.O. (2008). Inhibitory receptor signaling via tyrosine phosphorylation of the adaptor Crk. Immunity *29*, 578–588.

Poli, A., Michel, T., Thérésine, M., Andrès, E., Hentges, F., and Zimmer, J. (2009). CD56bright natural killer (NK) cells: an important NK cell subset. Immunology *126*, 458–465.

Poznanski, S.M., and Ashkar, A.A. (2019). What Defines NK Cell Functional Fate: Phenotype or Metabolism? Front. Immunol. *10*.

Renedo, M., Arce, I., Rodríguez, A., Carretero, M., Lanier, L.L., López-Botet, M., and Fernández-Ruiz, E. (1997). The human natural killer gene complex is located on chromosome 12p12-p13. Immunogenetics *46*, 307–311.

Rini, J.M. (1995). Lectin Structure. Annu. Rev. Biophys. Biomol. Struct. *24*, 551–577.

Sancho, D., Santis, A.G., Alonso-Lebrero, J.L., Viedma, F., Tejedor, R., and Sánchez-Madrid, F. (2000). Functional Analysis of Ligand-Binding and Signal Transduction Domains of CD69 and CD23 C-Type Lectin Leukocyte Receptors. J. Immunol. *165*, 3868–3875.

Sancho, D., Gómez, M., and Sánchez-Madrid, F. (2005). CD69 is an immunoregulatory molecule induced following activation. Trends Immunol. *26*, 136–140.

Santis, A.G., Campanero, M.R., Alonso, J.L., Tugores, A., Alonso, M.A., Yagüe, E., Pivel, J.P., and Sánchez-Madrid, F. (1992). Tumor necrosis factor-α production induced in T lymphocytes through the AIM/CD69 activation pathway.

Santis, A.G., López-Cabrera, M., Sánchez-Madrid, F., and Proudfoot, N. (1995). Expression of the early lymphocyte activation antigen CD69, a C-type lectin, is regulated by mRNA degradation associated with AU-rich sequence motifs. Eur. J. Immunol. *25*, 2142–2146.

Schuck, P. (2000). Size-distribution analysis of macromolecules by sedimentation velocity ultracentrifugation and lamm equation modeling. Biophys. J. *78*, 1606–1619.

Sheard, M.A., Asgharzadeh, S., Liu, Y., Lin, T.-Y., Wu, H.-W., Ji, L., Groshen, S., Lee, D.A., and Seeger, R.C. (2013). Membrane-Bound TRAIL Supplements Natural Killer Cell Cytotoxicity Against Neuroblastoma Cells. J. Immunother. Hagerstown Md 1997 *36*, 319–329.

Shiow, L.R., Rosen, D.B., Brdičková, N., Xu, Y., An, J., Lanier, L.L., Cyster, J.G., and Matloubian, M. (2006). CD69 acts downstream of interferon-α/β to inhibit S1P1 and lymphocyte egress from lymphoid organs. Nature *440*, 540–544.

Smyth, M.J., Cretney, E., Kelly, J.M., Westwood, J.A., Street, S.E.A., Yagita, H., Takeda, K., Dommelen, S.L.H. van, Degli-Esposti, M.A., and Hayakawa, Y. (2005). Activation of NK cell cytotoxicity. Mol. Immunol. *42*, 501–510.

Stríz, I., and Trebichavský, I. (2004). Calprotectin – a Pleiotropic Molecule in Acute and Chronic Inflammation. *53*, 9.

Sun, J.C., and Lanier, L.L. (2009). Natural killer cells remember: An evolutionary bridge between innate and adaptive immunity? Eur. J. Immunol. *39*, 2059–2064.

Suto, Y., Yabe, T., Maenaka, K., Tokunaga, K., Tadokoro, K., and Juji, T. (1997). The human natural killer gene complex (NKC) is located on chromosome 12p13.1-p13.2. Immunogenetics *46*, 159–162.

Testi, R., D'Ambrosio, D., De Maria, R., and Santoni, A. (1994). The CD69 receptor: A multipurpose cell-surface trigger for hematopoietic cells. Immunol. Today *15*, 479–483.

Tomasello, E., Bléry, M., Vély, F., and Vivier, E. (2000). Signaling pathways engaged by NK cell receptors: double concerto for activating receptors, inhibitory receptors and NK cells. Semin. Immunol. *12*, 139–147.

Topham, N.J., and Hewitt, E.W. (2009). Natural killer cell cytotoxicity: How do they pull the trigger? Immunology *128*, 7–15.

Trowsdale, J. (2001). Genetic and functional relationships between MHC and NK receptor genes. Immunity *15*, 363–374.

Turvey, S.E., and Broide, D.H. (2010). Innate immunity. J. Allergy Clin. Immunol. *125*, S24–S32.

Vance, B.A., Wu, W., Ribaudo, R.K., Segal, D.M., and Kearse, K.P. (1997). Multiple Dimeric Forms of Human CD69 Result from Differential Addition of N-Glycans to Typical (Asn-X-Ser/Thr) and Atypical (Asn-X-Cys) Glycosylation Motifs. J. Biol. Chem. *272*, 23117–23122.

Vaněk, O., Nálezková, M., Kavan, D., Borovičková, I., Pompach, P., Novák, P., Kumar, V., Vannucci, L., Hudeček, J., Hofbauerová, K., et al. (2008). Soluble recombinant CD69 receptors optimized to have an exceptional physical and chemical stability display prolonged circulation and remain intact in the blood of mice. FEBS J. *275*, 5589–5606.

Varki, A., Etzler, M.E., Cummings, R.D., and Esko, J.D. (2009). Discovery and Classification of Glycan-Binding Proteins. In Essentials of Glycobiology, A. Varki, R.D. Cummings, J.D. Esko, H.H. Freeze, P. Stanley, C.R. Bertozzi, G.W. Hart, and M.E. Etzler, eds. (Cold Spring Harbor (NY): Cold Spring Harbor Laboratory Press), p.

Vazquez, B.N., Laguna, T., Carabana, J., Krangel, M.S., and Lauzurica, P. (2009). CD69 Gene Is Differentially Regulated in T and B Cells by Evolutionarily Conserved Promoter-Distal Elements. J. Immunol. *183*, 6513–6521.

Vilches, C., and Parham, P. (2002). KIR: diverse, rapidly evolving receptors of innate and adaptive immunity. Annu. Rev. Immunol. *20*, 217–251.

Vivier, E., Tomasello, E., Baratin, M., Walzer, T., and Ugolini, S. (2008). Functions of natural killer cells. Nat. Immunol. *9*, 503–510.

Voskoboinik, I., Whisstock, J.C., and Trapani, J.A. (2015). Perforin and granzymes: function, dysfunction and human pathology. Nat. Rev. Immunol. *15*, 388–400.

Weis, W.I., Taylor, M.E., and Drickamer, K. (1998). The C-type lectin superfamily in the immune system. Immunol. Rev. *163*, 19–34.

Zamai, L., Ahmad, M., Bennett, I.M., Azzoni, L., Alnemri, E.S., and Perussia, B. (1998). Natural Killer (NK) Cell–mediated Cytotoxicity: Differential Use of TRAIL and Fas Ligand by Immature and Mature Primary Human NK Cells. J. Exp. Med. *188*, 2375–2380.

Zelensky, A.N., and Gready, J.E. (2005). The C-type lectin-like domain superfamily. FEBS J. *272*, 6179–6217.

Svoluji k zapůjčení této práce pro studijní účely a prosím, aby byla řádně vedena evidence vypůjčovatelů

Jméno a příjmení s adresou	Číslo OP	Datum vypůjčení	Poznámka